Diploma Thesis

Central Institute for Medical Technology,

Technical University of Munich

and

Cardiovascular Research Unit,

University of Cape Town

Cand.-Ing. Aurelia Herrmann
Matriculation number: 2310258
Course of Study: Mechanical Engineering

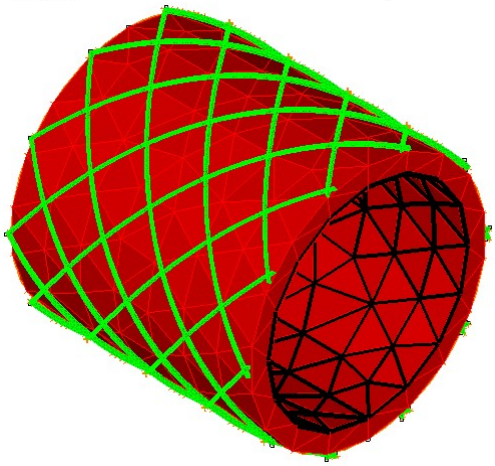

Supervisor: Dr. Thomas Franz, Michael Stöver
Partner: UCT
Distributed on: 1st November 2005
Gave in: 1st May 2005
Garching, 1st May 2005

....
Michael Stöver Aurelia Herrmann

Diploma thesis

Central Institute for Medical Technology,
Technical University of Munich
and
Cardiovascular Research Unit,
University of Cape Town

Numerical modelling of cardiovascular prostheses incorporating Nitinol structures

Important factors for the durability of cardiovascular prostheses are design, choice and combination of materials which are used for their components. This study involved the development of a Finite Element analysis tool to simulate and predict the mechanical behaviour of helical and braided tubular structures comprising Nitinol wires for the use in cardiovascular prostheses. In particular, the effect of stress and compliance depending on the prosthesis design is analysed and presented. Experimental tensile tests were performed at physiological temperature to determine the mechanical properties of the Nitinol. Subsequently, the data was used as input for the FE material model. FE analysis of tensile tests of Nitinol wires was performed. The numerical results were verified with the experimental data with regard to constitutive material model and FE model. 3-D geometrical models of the Nitinol structures were created in Pro/Engineer Wildfire, converted and imported into ADINA, Finite Element Analysis software, to establish the FE models. A constitutive material model for shape memory alloys was employed to describe shape memory and superelastic properties of Nitinol. The analysis of tubular Nitinol structures was conducted with FE models comprising the Nitinol structure, a tubular Latex structure, a fluid model, and fluid-structure interaction. A normal traction was applied to the fluid mesh approximating the blood pressure profile of a cardiac cycle. The analysis of the numerical results of the FE models was focused on stress and compliance analysis to determine the mechanical behaviour depending on different Nitinol design structures.

Affidavit

The author hereby certifies that she has independently written this document. All sources used have been indicated as references and no knowledge of other origin has been incorporated into this thesis. This diploma thesis has not been submitted to any other institution for the fulfilment of academic requirements.

Garching bei München, April 30th , 2005

Aurelia Herrmann

Acknowledgement

I would like to express my enormous thanks to:

Prof. Dr.med Peter Zilla and *Prof. Dr. med. Dr.-Ing. habil. Erich Wintermantel*, who have given me the opportunity to do research for this Diploma thesis in the Cardiovascular Research Unit (CVRU) at University of Cape Town.

Dr. Thomas Franz, who was a great supervisor and guided me to the end of my work.
I am deeply appreciative for his personal coaching and his openness in discussing various problems.

Dipl.-Ing. Michael Stöver for his support at home and grading the thesis.

Furthermore, I would like to thank my colleagues, in particular Helena van der Merwe, from the CVRU for the friendly and inspiring working atmosphere at the institute.

Also, I am most grateful to the DAAD (Deutscher Akademischer Austausch Dienst) for financially supporting my stay in South Africa.

Finally I would like to thank my parents, my boyfriend and my friends who supported and encouraged me during the preparation of this work and throughout my university career.

Contents

List of Medical Definitions

Adventitia	Outermost layer of a blood vessel
Anastomosis	The surgically connection of two ends of a blood vessel to form a continuous channel conduit end-to-end, end-to-side, side-to-side
Arteriosclerosis	Disease of the arteries characterized by the thickening or hardening of the arterial walls caused by fatty or calcium deposits in the artery walls
Bypass	A surgical procedure designed to increase blood flow to an organ or extremity that has narrowing or blockage of the blood supplying artery
Compliance	The percentage diameter or volume change (diametric or volumetric compliance) of a blood vessel per unit change in internal pressure.
Intima	Innermost layer of a blood vessel
Media	Mid-layer of blood vessel wall
Windkessel effect	The elastic expansion and return of arteries aiding the steady flow of blood

List of Mechanical Definitions

Austenite	The high-temperature phase of shape memory alloy
Biocompatibility	The suitability of a material for use in the human body and in endogenous fluid
Finite element analysis	A computer based analysis method which calculates the theoretical response of the model by solving a set of simultaneous equations that represent the behaviour of the structure under loading
Hysteresis	The temperature difference between a phase transformation upon heating and cooling.
Martensite	Low-temperature phase of shape memory alloy
Nitinol	Common trade name for the commercially most important family of shape memory alloy, Nickel-Titanium alloys
Superelasticity	The ability of an alloy specimen to return to its original shape upon unloading after a substantial deformation due to stress-induced phase transformation
Shape memory alloy	Material with an ability to return to some previously defined shape or size when subjected to an appropriate thermal procedure
Transformation temperature	Temperature of the start and finish of the phase transformation (M_s, M_f, A_s, A_f)

List of Tables

List of Figures

1 Introduction

1.1 Motivation

Arteriosclerosis with its fatal subsequential diseases such as heart attack and stroke is still the most common cause of death in the western world [1]. Arteriosclerosis is a disease of the arteries in which atherosclerotic plaques are formed in the vessel wall and in late stages may reduce or restrict blood flow in the lumen. It becomes seriously symptomatic when interfering with the coronary circulation supplying the heart or cerebral circulation supplying the brain. Conservative medical treatment, drug therapy, doesn't suffice anymore and interventional or operative therapies like cardiovascular prostheses, angioplasty or Coronary artery bypass grafting (CABG) have to be carried out.

Important factors for the durability of cardiovascular prostheses are design, choice and combination of materials which are used for creating their components. The development of cardiovascular prostheses undergoes several iteration steps which can be very time consuming to guarantee the desired material behaviour. Therefore, numerical simulation methods have been established as one of the most important tool in the product development process. In particular, the Finite Element Method deals with complex structures and materials and allows the designer to predict the mechanical behaviour and to optimise the design of his products.

The Cardiovascular Research Unit at the University of Cape Town (UCT), South Africa, has focused on research and development of cardiovascular prostheses and its optimisation. The primary aim is to obtain cardiovascular devices with desired materials so that an optimal adaptation to the original physiological condition can be achieved. The approximation of the mechanical behaviour of the prostheses compared to the mechanical behaviour of native vessel tissue has to be guarantied.

1.2 Purpose

The aim of the project was to numerically model (using Finite Element Modelling) the mechanical behaviour of structural components of vascular prostheses comprising various synthetic materials. 3-D Fluid-Structure Interactions (FSI) Models, created and solved by the Finite Element software ADINA, were used to simulate and analyse the mechanical behaviour of helical and braided tubular structures comprising thin Nitinol wires for the use in cardiovascular prostheses. In particular the effect of stress and compliance depending on the device design is analysed. Thus, it is anticipated that the models could be potentially used for future design optimisation of cardiovascular prostheses prior to costly prototype studies.

1.3 Procedure

For this thesis the following steps were performed:

- Literature review
- Experimental testing
- Development of Finite Element models in ADINA
    - Implementation and adaptation of required material models
        - Integration of the SMA user-supplied material model
        - Application of the latex material model
        - Application of fluid material model
    - Geometry modelling of components of the device
        - Geometry modelling of the SMA wire tensile test
        - Geometry modelling of the helical reinforcement Nitinol structure
        - Importing and generating the braided stent structure
        - Geometry modelling of the latex liner
        - Geometry modelling of the fluid model
    - Assembly of the structural and material components
    - Defining contact mechanism
    - Defining the Fluid-Structure-Interaction
- Simulation of various load cases of different complexity
    - Tensile Test
    - Transient pulsatile pressure flow
- Verification of numerical models and results
    - Verification of FEM wire tensile test by experiment wire tensile tests
    - Verification by literature value comparison
- Validation of the Finite Element models

2 Theory

This work is multi-disciplinary in nature and requires understanding of various disciplines. This chapter focuses on introducing the basics in biology and medicine of human vessels, in shape memory materials and in Finite Element Methods which are required for understanding the study.

2.1 The human blood vessels

The circulatory system of the human body delivers oxygen and nutrients throughout the body by a complex network of vessels. Arteries, arterioles and capillaries carry blood to all parts of the body and allow exchange of nutrients and wastes through capillary walls from blood to the tissues and organs. Veins carry deoxygenated blood back to the lungs for reoxygenation.

The majority of the cardiovascular prostheses are used to supply deficiencies of arteries. Therefore, the mechanical behaviour of arteries is required to understand the mechanical loads of cardiovascular prostheses.

2.1.1 Anatomy of arteries

Arteries are roughly subdivided into elastic and muscular types. Elastic arteries have large diameters and are located close to the heart (for example the aorta). Muscular arteries are located at the periphery. Their diameters are smaller than 0.1 mm [2]. The structure of arterial walls consists of three different layers (see Fig 2.1):

1. Intima (tunica intima)
2. Media (tunica media)
3. Adventitia (tunica externa)

The properties of each of these layers will be discussed briefly:

The intima is the innermost layer and generally consists of endothelial cells and rests on a thin basal membrane (basal lamina). The thickness of the endothelial cells is about 0.2-0.5μm [2]. In healthy young muscular arteries, the intima is a very thin and its influence on the mechanical properties of the arterial wall is ignorable. Depending on the age the thickness and stiffness of the intima can increase (arteriosclerosis) so that the mechanical influence can be more significant.

The middle layer of the artery, the media, consists of a complex three-dimensional network of smooth muscle cells, elastin and collagen fibrils [3]. The elastic laminae separate the media into varying number of well-defined concentrically fibre-reinforced medial layers. The inter-

nal and external elastic laminae separate the media from the intima and adventitia. The orientation of the interconnection of the elastic and collagen fibrils, the elastic laminae and the muscle cells together build a continuous fibrous helix. Due to this structural order, the media has a high strength and elasticity in longitudinal and circumferential direction. Therefore, the influence of the media on the mechanical behaviour of arterial walls is most significant.

The adventitia, the outermost layer of the artery, consists of fibroblasts, fibrocytes, bundles of collagen fibrils and a ground substance. The thickness of the adventitia depends on the type (elastic or muscular) and on the physiological function of the artery [3]. The collagen fibrils are arranged in helical structures and reinforce the artery wall. The adventitia is surrounded by a loose connective tissue. Concerning the influence on the mechanical behaviour of the artery wall, the adventitia is less stiff than the media. However the adventitia has a significant influence on the stability and strength of the wall and prevents the artery from overstretching and rupturing at higher pressure.

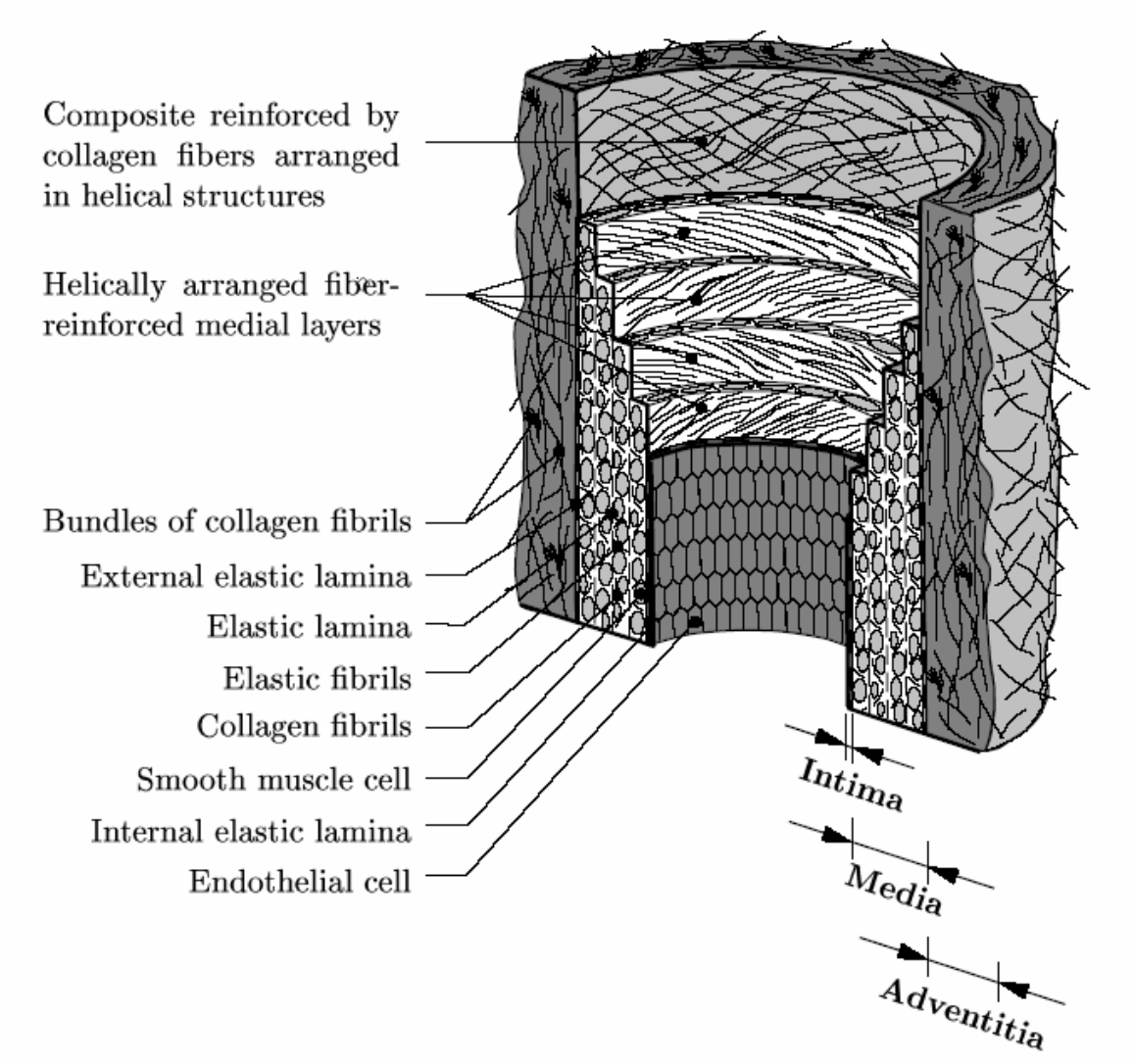

Fig 2.1: Microscopic structure of a healthy elastic artery. The three layer, intima, media and adventitia are presented. The components of each layer can be seen in the figure. (Modified from [3])

2.1.2 Mechanical behaviour of arteries

The mechanical behaviour of arteries is complex as a result of their composite structure. The most important mechanical properties of arteries are as follow:

- Non-linear: Artery shows non-linear behaviour on the pressure-strain graph (see Fig 2.2).
- Viscoelastic: Artery tissue arteries exhibit hysteresis under cyclic loading, as shown in Figure 2.2
- Anisotropic: The mechanical behaviour is different in different directions because of the layered structure of the artery wall (see Fig 2.1)
- Incompressible [4]
- Pre-stressed (longitudinally and circumferentially) when no internal pressure is present [4]

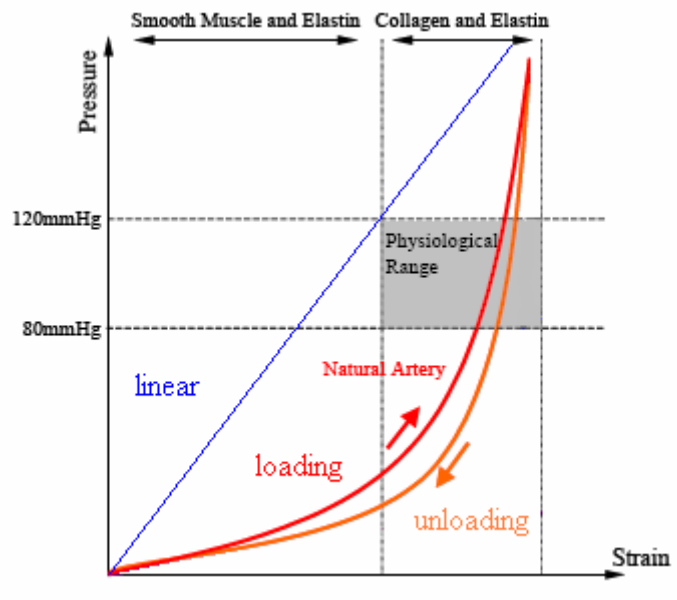

Fig 2.2: Pressure-strain relationship of an artery showing hysteresis between the loading and unloading. (Modified from Yeoman [5])

The difference between systolic and diastolic pressures generates the most significant forces in the arteries. The vessel dilation caused by these pressures is an important physical characteristic of the arterial system. The compliance of arteries have been measured, both in vitro using excised sections of vessel, and in-vivo non-invasively with ultrasonic techniques [6]. Generally the compliance can be expressed as diameter compliance C_d and volume compliance C_v.

These are defined by

$$C_d = \frac{\Delta d}{d_{dia}\Delta P} \times 100 \times 100\, mmHg \tag{2.1}$$

$$C_v = \frac{\Delta V}{V_{dia}\Delta P} \times 100 \times 100\, mmHg \tag{2.2}$$

where d_{dia} and V_{dia} are the internal diameter and internal volume of the vessel at the diastole. ΔP is the pressure difference between systolic and diastolic pressure. Δd and ΔV are the change in diameter and volume induced by this pressure difference. Compliance is expressed in percentage change of diameter or volume over 100mmHg pressure (%/100mmHg). [5]

There are two ways to characterise the compliance of a vessel: static and dynamic compliance. Static compliance testing involves the step-wise increase in internal pressure and a consequential diameter change. The disadvantage of this method is that it does not describe the strain rate effects on the vessel, which may have a influence on compliance. If the material is viscoelastic, at higher strain rates the material will appear "stiffer", due to slow strain response [5]. Dynamic compliance testing is carried out under pulsatile pressure conditions over a period of time. However, depending on the time, fast step-wise pressure change can be similar to pulsatile pressure conditions.

An other important parameter to describe the elasticity of vessel wall is the pressure–strain elastic modulus, K. This is defined as

$$K = \frac{d\Delta P}{\Delta d} \tag{2.3}$$

and is the inverse of diameter compliance. The pressure-strain elastic modulus K is measured in mmHg or Pa.

Comparing the two mechanical properties, compliance and pressure-strain elastic modulus, to the common used mechanical parameter to describe elasticity, the following difference is indicated. In contrast to Young's modulus, neither the pressure–strain elastic modulus nor compliance coefficients require the measurement of arterial wall thickness which is a difficult measurement to perform in vivo [6].

2.2 Cardiac cycle

2.2.1 Pressure and flow in arteries

Due to the pump action of the heart, a pressure pulse is created within the blood vessels of the body. The upper bound of pressure is reached in the systole and the lower bound in the diastole. Figure 2.3 shows the typical pressure and flow waves in the arterial tree for an average adult human. The shape of the pressure wave and the systolic and diastolic pressure values depend on the position of the artery in the body. Regarding an adult, the systolic and the diastolic pressures of the ascending aorta can range from 100-150mmHg to 60-100mmHg [5].

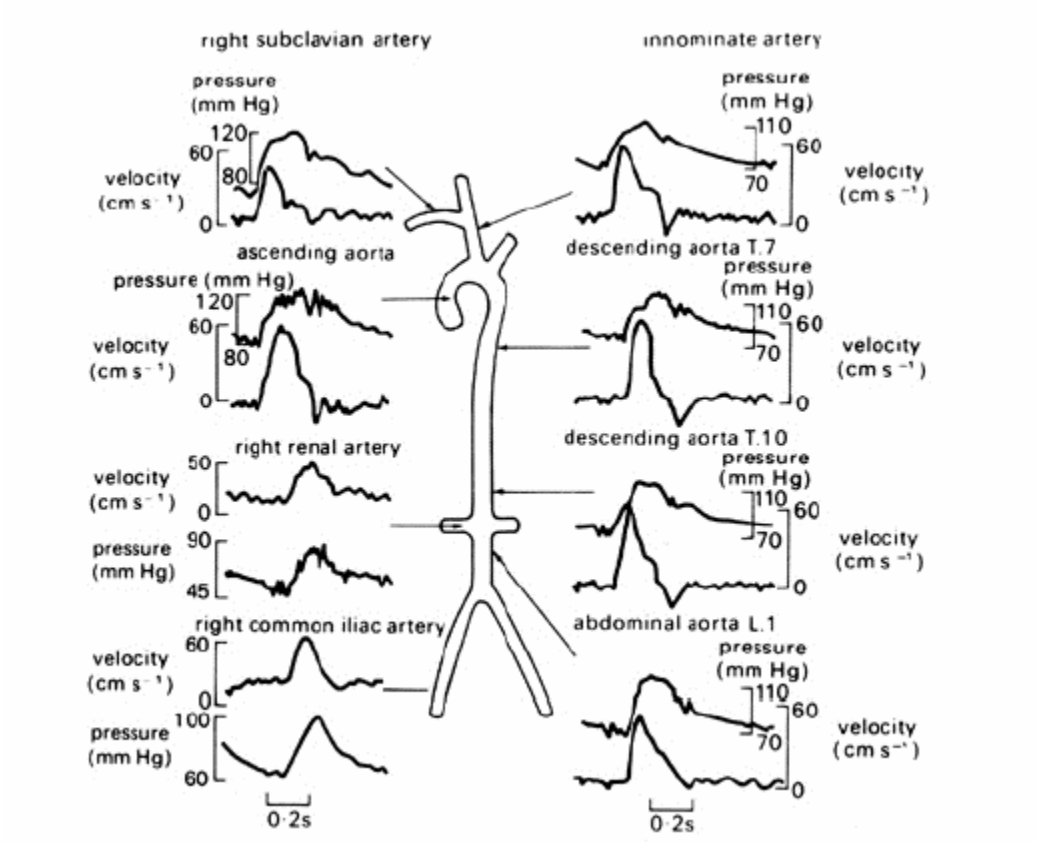

Fig 2.3: Pressure and flow waveforms in the human artery system. The velocity and the pressure depends on the position of the artery in the body. [7]

2.2.2 Mathematical approximation of transient pulsatile pressure

A six-term Fourier series serves as a mathematical approximation of transient pulsatile pressure of one cardiac cycle and is given as

$$f = A_0 + \sum_{1}^{n} (B_n \sin nw(t - t_0)) \text{ for } t \geq t_0 \tag{2.4}$$

$$f = A_0 \text{ for } t \leq t_0 \tag{2.5}$$

with n describes the number of terms ($n = 6$). The frequency is given for the period of one heart beat, $T = 0.83s$, as $w = \frac{2\pi}{T} = 7.5 rad / \sec$. The time at which cyclic load starts is $t_0 = 0$. The initial amplitude is $A = 13332 \text{ Pa}_0$ [5].

The Fourier series constants B_n are given as
$B_1 = 2418.5$, $B_2 = 691.0$, $B_3 = 230.33$, $B_4 = 115.17$, $B_5 = 114.7$ and $B_6 = 114.7$

Figure 2.4 presents the comparison of the Fourier model with the proximal, distal and average physical pressure curves.

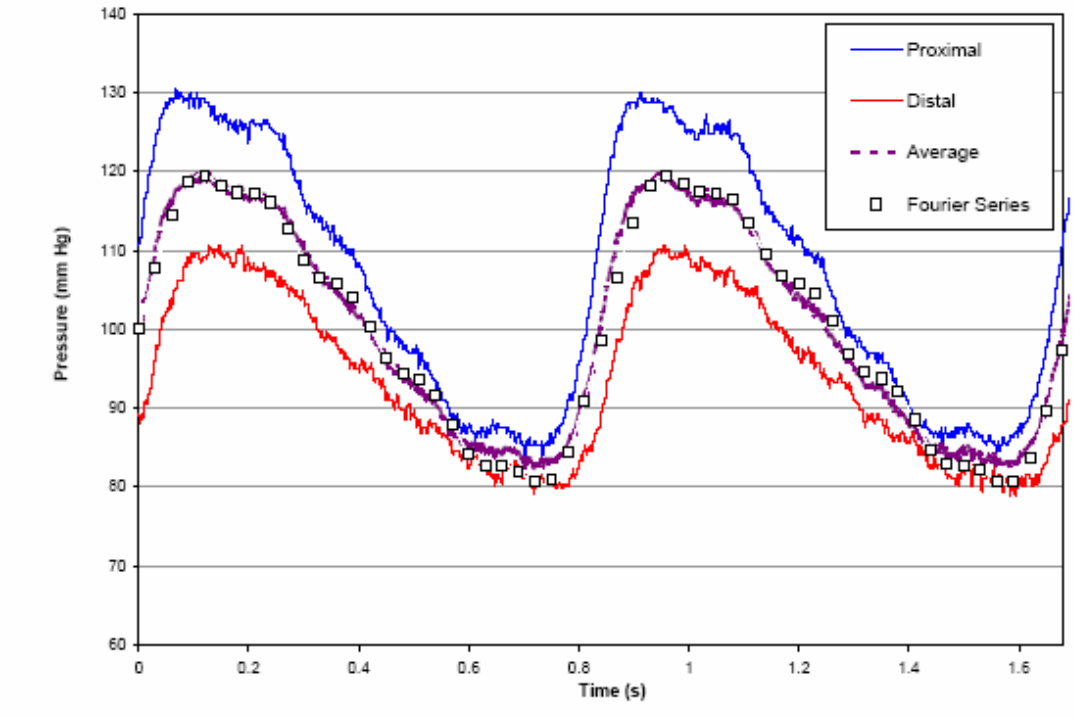

Fig 2.4: Comparison of the Fourier model with physical pressure curves [5]

2.3 Shape Memory Alloys in cardiovascular prostheses

2.3.1 Design of cardiovascular prostheses

The success of cardiovascular prostheses depends on its mechanical behaviour corresponding to the mechanical properties of host native vessel tissue. In the last years, much effort by medical technology companies like Medtronic has been carried out on prostheses design (e.g. stent structures) and material optimisation. The prosthesis's long term ability to function in the circulatory system is still a challenging aim in the medical technology field. Important critical tasks in the development process of cardiovascular prostheses are [5]:

- The correct matching the mechanical properties of the prostheses to those of the host vessel
- The biological reaction of the synthetic materials to the native vessel tissue concerning rejection for example.
- The reduction of stress across the anastomosis
- The reduction of the blood flow disruptions

The matching of the mechanical properties of the prostheses to the host vessel is an important aspect for the success of the prostheses. One important mechanical property to consider is the compliance. The compliance of the artery has an influence on the blood flow through the artery. Achieving a similar compliance of the prostheses compared to those of the artery reduces thrombosis build up, allows for a steady transfer of the pressure pulse and windkessel effect [8] and reduces the elastic stress-strain difference between the prostheses and the host artery.

The compliance of the prostheses depends on the design and material combination of the components. Various metal alloys like stainless steel or shape memory alloys are used to create the structure of cardiovascular prostheses. Shape memory alloys are one of the most interesting materials for this medical application.

2.3.2 Shape Memory Alloys and their characteristics

Due to the unique mechanical properties and to its biocompatibility, shape memory alloys (SMA) have found a great field of medical use. There are different compositions of SMA for example Ag-Cd, Au-CD, Cu-Zn-Al, Ni-Al and NiTi [9]. The most often used SMA in medical world is Nitinol (about 50% Nickel and 50% Titanium). It has its name because of its discovery at the US Naval Ordnance Laboratory (Nickel Titanium Naval Ordnance Laboratory) in the early 1960 [10]. Biocompatibility, Superelasticity effect and Shape memory effect capabilities, and the temperature range of Nitinol's superelasticity which includes human body

temperature are some of advantages of this SMA. Therefore, Nitinol serves as a common application in medical devices such as vascular stents, filters and surgical tools.

The mechanical properties can be explained by its microstructure. SMA has two stable solid phases at different temperatures: The martensite phase (M) is the low-temperature phase, which allows the metal to be soft and ductile (see Fig.2.5). Martensite has a monoclinic crystal structure in several variants (Variants are region of martensite with one assigned orientation like twined and ordered) [9]. The austenite phase (A) is the high-temperature phase. The Austenite lattice is made of with body-centred cubic ordered atoms which makes the metal hard and rigid [11]. The temperature range of the two phases is limited by start and finish temperature of the particular phase (see Fig.2.6).

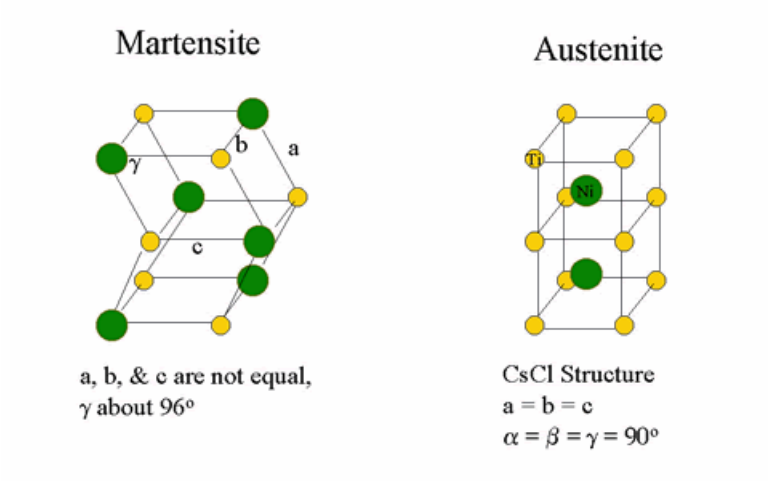

Fig 2.5 Comparison of the lattice structure of the two solid phases of Shape memory alloys [12]

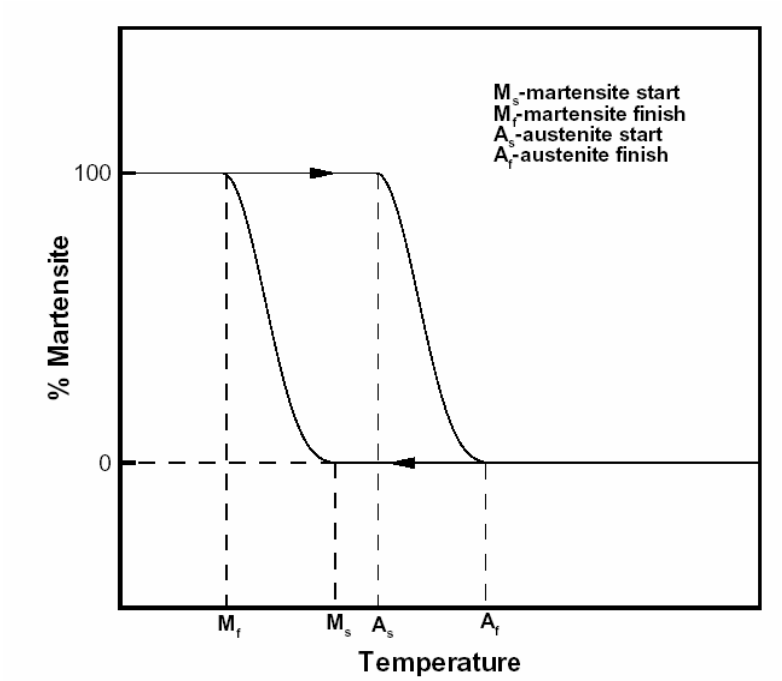

Fig 2.6 Presentation of the phase-transformation and -retransformation temperatures [13]

Two main effects, mechanical Superelasticity (SE) and thermal Shape Memory Effect (SME), can be achieved depending on material composition, heat treatment, constitutive temperature and applied forces.

2.3.2.1 Superelasticity effect

The Superelasticity (SE) of memory alloys is based on a transformation of the crystal structure, from austenite to martensite, if mechanical loads affect the material (see Fig.2.5). During unloading and when the temperature is above the temperature $T = A_f$, the phase retransforms. After undergoing a hysteresis stain-stress loop (this effect is named as pseudoelasticty), the material recovers to its initial shape and austenite structure (see Fig. 2.7). Due to the fact that the transformation strains are large (of order of 6-8%) compared to the typical elastic strains in a metal, the material is said to be superelastic.

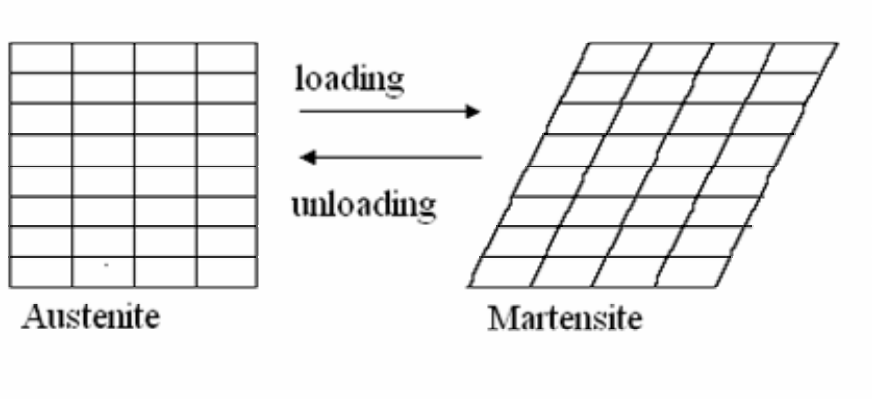

Fig 2.7 Transformation of crystal structure between austenite and martensite

Figure 2.8 shows the schematic illustration of the superelastic effect with its typical stress-strain curve. The first elastic deformation shows a great stress increase over a small strain range, $\Delta\varepsilon_1$. Following this initial deformation, the curve plateaus with little change in stress for a much larger strain range, $\Delta\varepsilon_2$, are presented. On this plateau, martensite laths nucleate and grow with the preferred martensite variant. After the martensitic transformation is complete, elastic deformation continues over the strain range, $\Delta\varepsilon_3$, until yielding of the martensite or unloading. When the stress is decreased, the reverse process is observed. After elastic recovery over $\Delta\varepsilon_3$, the plates which formed during loading over $\Delta\varepsilon_2$ revert along the previous crystallographic path. The volume fraction of martensite decreases over $\Delta\varepsilon_4$. This is the process by which the parent phase is recovered, so the original undeformed material is restored.[14]

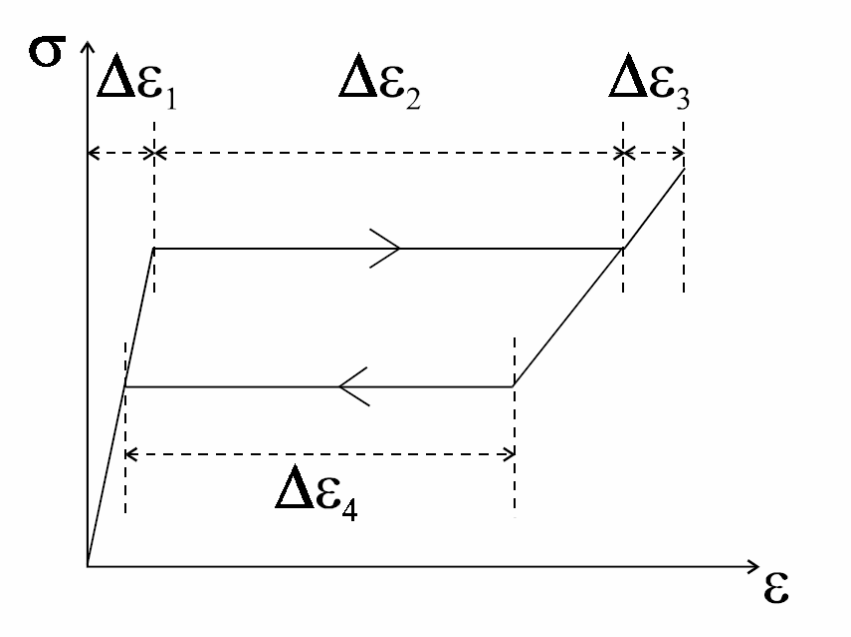

Fig 2.8 Schematic illustration of the superelastic effect its typical stress-strain curve. Four characteristic strain ranges are presented.[14]

2.3.2.2 Shape memory effect

The second effect, the thermal Shape Memory Effect (SME), is obtained by temperature changes and is split in two effects: One-way and two-way SM effect.

One-way effect

The crystal structure in the martensite phase is characterized by the fact that the atoms can be in a "twin structure" or in ordered martensite. After deforming the material, its martensite-twin shape transforms to ordered martensite and remains in this stage, even the unloading is completed. Upon heating, a phase transformation from ordered martensite to austenite is performed. After cooling, the previously deformed body recovers the initial shape (see Fig.2.9). A retransformation from austenite to martensite-twin is observed.

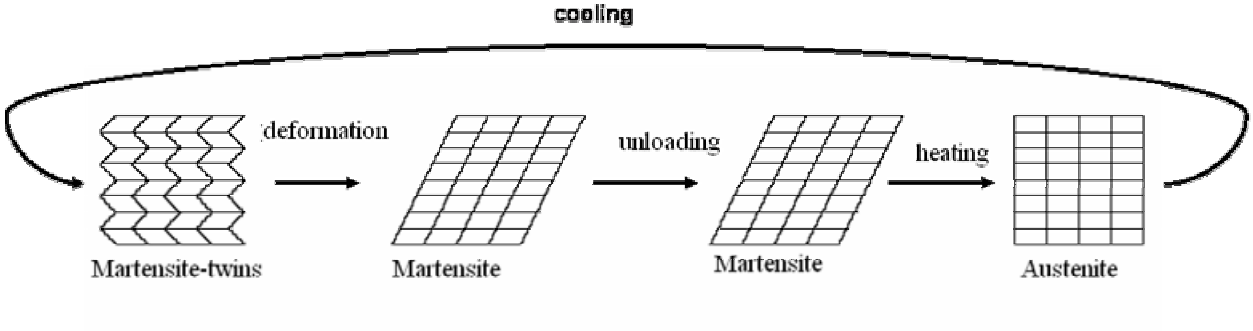

Fig 2.9 Schematic description of the one way shape memory effect

Figure 2.10 presents the one-way shape memory effect on the basis of an austenite sample which is cooled through the martensitic transformation to a temperature below the martensite finish temperature, M_f. At this point the sample is deformed to within ~10% strain. After unloading, the sample is heated through the martensite to austenite transformation. The martensite laths revert to austenite along the original paths, such that the deformation previously applied disappears as the temperature is increased. At A_f the strain is completely recovered, and the material has the same original shape before the deformation portion of the cycle.[14]

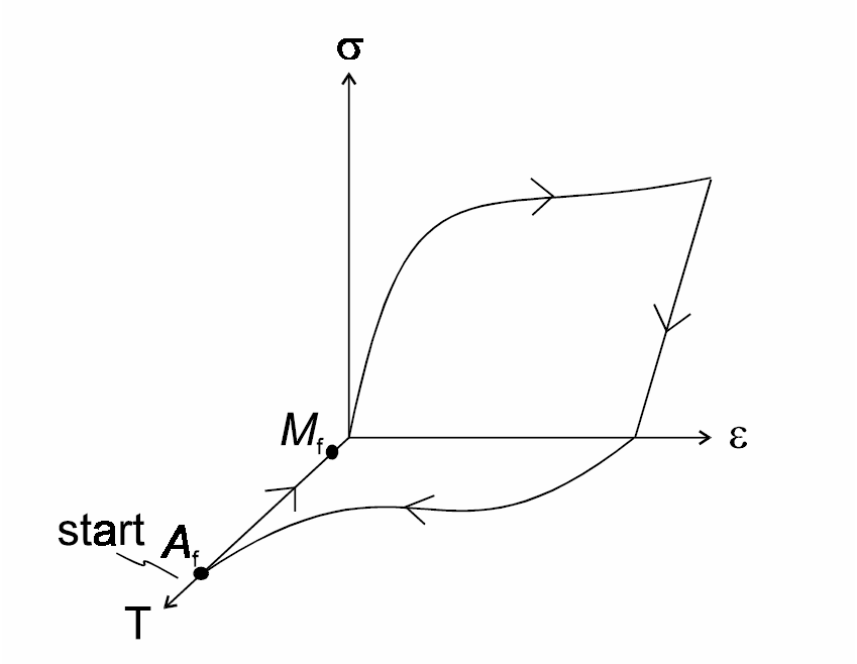

Fig 2.10 Schematic illustration of the shape-memory effect on the basis of an austenite sample which undergoes a transformation and re-transformation back to its original shape. [14]

Two-way effect

The retransformation from austenite to martensite-twin, as described above, is not implemented if internal structure stresses or mechanical loads exist. Temperature change causes a transformation between ordered martensite and austenite. Because of permanent micromechanical defects inside the structure, the material will not redeform to original martensite-twin stage after cooling. However, this effect can be in the interest of recovering a specific shape upon heating and then return to an alternate shape when cooled. There are limitations that reduce the usability of the two-way effect, such as smaller strains (2 %) and unknown, long-term fatigue and stability. Additionally, setting shapes in two-way SMA is a more complex procedure than the one used with one-way SMA. The two-way effect is not used in the creation of cardiovascular prostheses which are described in this work.

Figure 2.11 illustrates the cyclic change between ordered martensite and austenite and demonstrates the two-way shape memory effect.

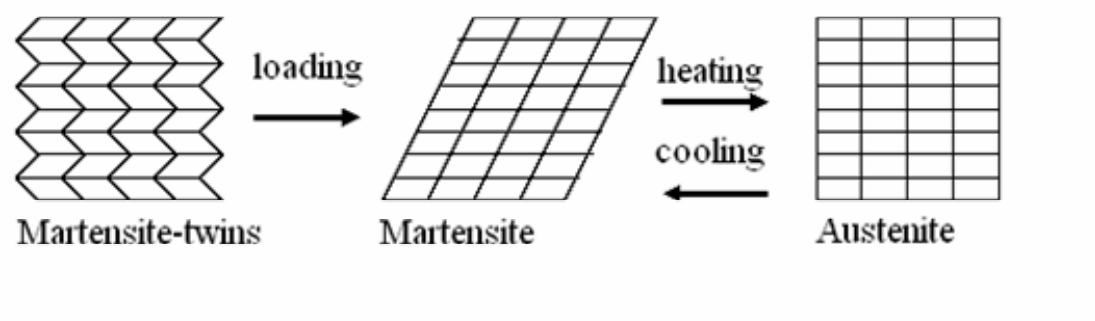

Fig 2.11 Schematic description of the two-way shape memory effect

2.4 The Finite Element Method

2.4.1 Introduction to FEA

Finite element analysis (FEA) is a numerical technique that allows users to calculate how a field (e.g. displacement, temperature, velocity) can vary in space within a particular geometry. Since the computer efficiency, power and memory capacity have improved over the last few decades, the level of complexity of problems has increased, particularly concerning the geometrical presentation and material behaviour of the physical problems [15].

A complete Finite Element Analysis consists of three stages: preprocessing, simulation, and postprocessing (see Fig 2.12).

Preprocessing:
The first steps of any finite element simulation are to represent the physical problem by a mathematical model or idealization. That means that the material properties in the geometry and the environment around the geometry (boundary conditions, applied loads) must be expressed mathematically [15]. The actual geometry of the structure is then discretize using a collection of finite elements. Each finite element represents a discrete portion of the physical structure. The finite elements are joined by shared nodes. The collection of nodes and finite elements is called the mesh.

Simulation:
In a stress analysis the displacements of the nodes are the fundamental variables that an FE software program calculates. Once the nodal displacements are known, the stresses and strains in each finite element can be determined. The simulation is the stage in which the Finite Element Package solves the numerical problem defined in the model and stores the output files ready for postprocessing.

Postprocessing:
Once the solution is completed, the next step is to analyse the results with a postprocessing module of the FEM software package. The values of the field variables at all nodes or other physical parameter calculated on the basis of the field variables, are listed or graphically displayed. The visualisation of the results severs to understand and to interpret the results. An error analysis serves to analyse the computed results critically and to make decisions of their accuracy.

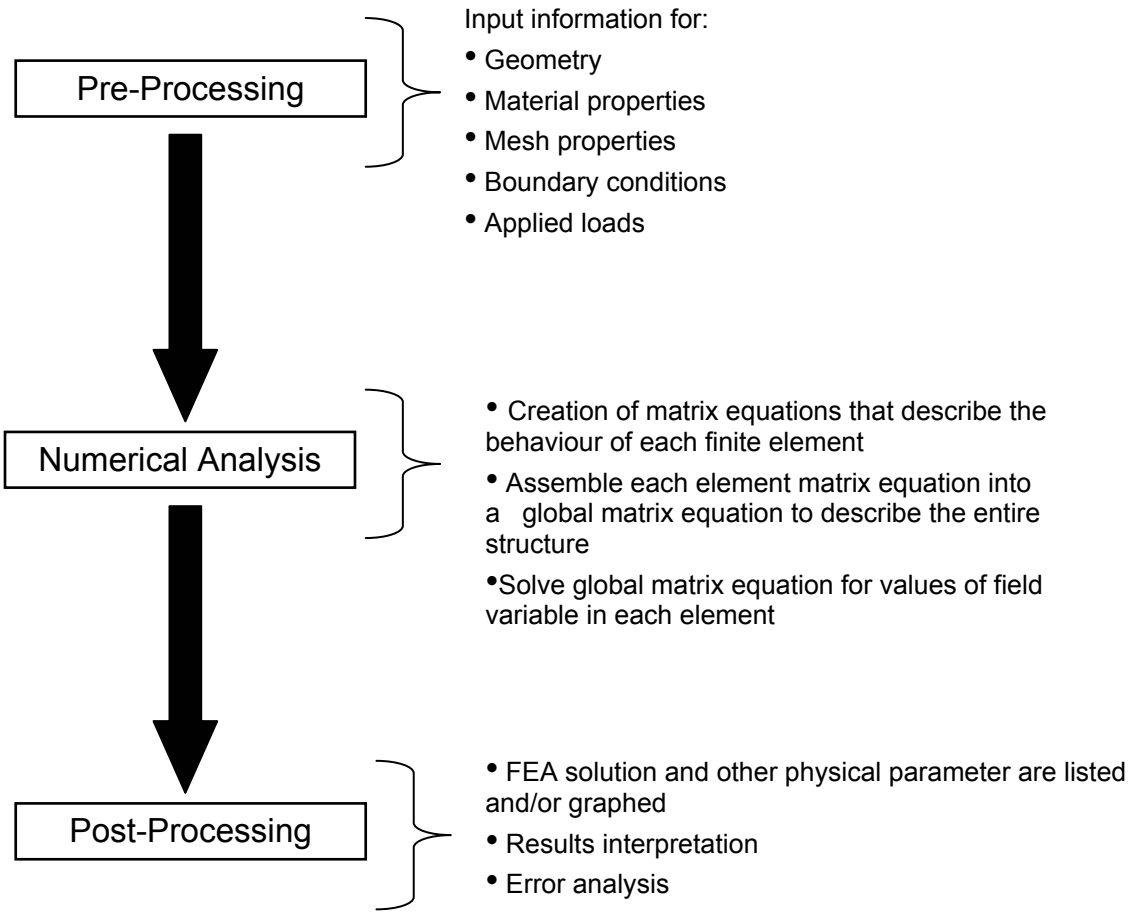

Fig 2.12 Schematically description of complete Finite Element Analysis. Representing the three stages: preprocessing, simulation, and postprocessing. The main tasks of each stage are summarised. (Modified from Wayne [15])

The main advantage of FEM is that the performance of cardiovascular prostheses can be predicted without considerable costs associated with laboratory experimentation. FEM analyses can be carried out before prototype are manufactured, and therefore, reduces the development costs. However, performing a simulation, certain simplifying assumptions have to be made. Thus, simulation is an approximation to describe real problems and it is considered as complement to experimental tests.

2.4.2 FEA material models

FE models predict mechanical behaviour of components of vascular prostheses. The material models need to be implemented and adapted for the components of the simulation FE models of vascular prostheses required for this work (hyperelastic rubber material, SMA and fluid). The FE software package ADINA is used for this work. The understanding of definition and integration of material models in the FE program is necessary. Therefore, the following sections concentrate on giving an overview of relevant information of the material models which have to be defined in ADINA. The procedure of the implementation and adaptation of materials might be different in other FE software packages.

2.4.1.1 User-supplied material model for shape memory alloys

The user-supplied material model is provided in ADINA to define any type of material model for use with 2-D or 3-D solid elements. The constitutive relation must be arranged in the form of an algorithm and implemented into subroutine CUSER2 for 2-D solid elements or into subroutine CUSER3 for 3-D solid elements.

Meissner [9], developed a numerical constitutive model of the non-linear thermo-mechanical behaviour of SMA for the use in Finite Element (FE) analysis and in particular in ADINA. The three-dimensional model based on a simplified constitutive law provides the possibility to calculate stressor temperature-induced forward and reverse phase transformations and uniaxial re-orientation of martensite variants. Several of the features of SMA are included: the shape memory effect by transformation, the shape memory effect by re-orientation, the pseudoelasticity effect and combined effects. The constitutive model for SMA is described in detail in [9].

For the application of the SMA material model the FORTRAN code of his model must be incorporated in the system files of ADINA. Detailed information about the process can be found in Appendix B.
For the use of the SMA material model the following 13 parameter are to be specified for the material:

E_a	Young's modulus of austenite
ν_a	Poisson ratio of austenite
E_m	Young's modulus of martensite
ν_m	Poisson ratio of martensite

C_a	Austenite transformation constant
C_m	Martensite transformation constant
A_s	Austenite start transformation temperature
A_f	Austenite end transformation temperature
M_s	Martensite start transformation temperature
M_f	Martensite end transformation temperature
C_r	Re-orientation constant
σ_r	Re-orientation stress limit
ε_l	Maximum transformation strain

2.4.1.2 Hyperelastic rubber material – Latex model

The mechanical behaviour of latex and soft tissue is described by a hyperelastic strain energy density function [3]. ADINA has two different material models available to describe rubber material and hyperelastic effects: Moon-Rivlin and Ogden. These material models can be employed with 2-D or 3-D solid elements and are qualified for large displacement or strain. The material models include hyperelastic and viscoelastic effects. For this thesis, the viscoelastic effects were neglected.

The Odgen model is compared to the Moon-Rivlin model a high order model (N=6) concerning the strain energy function which improves the correlation between experimental and numerical data [16]. The disadvantage of high order model is that a greater number of coefficients have to be fitted to experimental data. The Moon-Rivlin model is recommended by ADINA for analysis of biomechanical materials because of its orthotropic effects. In this work the Ogden material is used because its application to describe Latex material accurate was proved in [5].

The hyperelastic part of the Ogden model is based on the strain energy density equation:

$$W = \sum_{n=1}^{9} \left(\frac{\mu_n}{\alpha_n} \left[\lambda_1^{\alpha_n} + \lambda_2^{\alpha_n} + \lambda_3^{\alpha_n} - 3 \right] \right) \tag{2.6}$$

where μ_n and α_n are the Ogden material constants and $\lambda_1, \lambda_2, \lambda_3$ are the principal stretches. This strain energy funktion assumes an incompressible material and has to be modified for compressible, plane strain, axis-symmetric or 3-D analysis, respectively.

To define the Ogden material model a selection of material constants have to be done: Material constants μ_n, α_n and the bulk modulus. The material constants can be determined by curve-fit to experimental stress-strain data. The bulk modulus K is used to model the compressibility of material. With increasing the bulk modulus, the material will change toward incompressibility. ADINA [16] assumes a default for the bulk modulus based on small strain Young modulus E near incompressibility:

$$K = \frac{E}{3(1-2\nu)} \text{ with } \nu = 0.499 \tag{2.7}$$

with

$$E = \frac{3}{2}\sum_{n=1}^{9}(\mu_n \alpha_n) \ . \tag{2.8}$$

2.4.1.3 Fluid material model

ADINA-Fluid is used for analysing problems involving fluids. The fluids can be incompressible, slightly compressible and compressible flows, respectively, and flows in porous media. The problems can be modelled using either laminar or turbulent flow assumptions. Heat transfer and mass transfer can be incorporated. Additionally, solid models created in ADINA can be coupled with any fluid model for analysing fluid-structure interactions [16].

In fluid-structure interaction analyses, fluid forces are transferred to the solid and the solid deformation changes the fluid model. The computational model is divided into the fluid model and the solid model, which are defined by the respective material data, boundary conditions, etc. The interaction occurs along the interface of the two domains.

The basic conditions applied to the fluid-structure interfaces are the kinematical condition. The underlining of the values expresses that the values are defined only for the fluid-structure interfaces. The displacement of the fluid $\underline{d}_f$, is compatible to displacement of the solid $\underline{d}_s$:

$$\underline{d}_f = \underline{d}_s \tag{2.9}$$

Furthermore, dynamic conditions are applied to the fluid-structure interfaces. The stresses of the fluid f τ are equal to the solid stresses:

$$n \cdot \underline{\tau}_f = n \cdot \underline{\tau}_s \tag{2.10}$$

The fluid velocity condition is derived from the kinematical condition

$$\underline{v} = \dot{\underline{d}}_s \tag{2.11}$$

if a no-slip condition is applied, or

$$n \cdot \underline{v} = n \cdot \dot{\underline{d}}_s \,. \tag{2.12}$$

if a slip condition is applied. $\underline{v}$ describes the fluid velocity and $\dot{\underline{d}}_s$ is the derivation of the displacement of the solid $\underline{d}_s$.

In steady-state analyses, the mesh velocities are always set to zero even the fluid nodal displacements are updated. Accordingly, the fluid velocities on the fluid-structure interfaces are zero.

The constant material model is the material model used in this work. All fluid properties are assumed to be constant of time. The required fluid properties for a non heat-transfer problem are:

μ = Fluid viscosity
ρ = Fluid density
κ = Bulk modulus of elasticity

3 Methods

3.1 Experimental SMA wire tensile test

The following five steps were performed in this work for realizing the wire tensile test:

1. Purpose
2. Experimental set-up
3. Constitutive equations
4. Program adjustment
5. Analysis of the data

3.1.1 Purpose

The aim of the experimental wire tensile test is to determine mechanical properties of Nitinol, used as input for a FEM user-subroutine material model for SMA. Additionally, the experiment is used to validate the FEM Nitinol material model results against relevant experimental data, confirming that the SMA material model can be used for further FE simulation. The experimental tests have to be carried out under, or close to, physiological conditions.

3.1.2 Experimental set-up

The tensile tests were performed on a tensile machine from INSTRON. It was utilised to obtain uniaxial tensile test data for the SMA wire structure. The Nitinol material used for tested wires is BB alloy Nitinol. Two lengths of the wires, l=100mm and l=40mm, were used for testing. The experimental set-up allows performing the tensile test in a heated water bath. During testing, the temperature of the environment (water) was fixed at 37 °C. Figure 3.2 shows the tensile machine and experiment set up of the wire tensile test.

The wire specimen was glued to an aluminium strip, at both ends, using two-component epoxy resin glue (see Fig.3.1). Subsequently, the aluminium strips were fixed in the clamps. The influence of the aluminium strip on the results is assumed to be neglected because the deformation is very smaller compared to that of the Nitinol. To ensure that the sample was located centrally in the clamp, a ruler was utilised to determine the central position on the clamp. The specimen was positioned in the water bath and attached to the tensile tester with the use of locking pins. A space holder ensures that the distance between the clamps allows the desired length of the testing sample. Experimental tests were performed for different wire samples. Table A.1 in Appendix A gives an overview of the tested wires and the testing conditions.

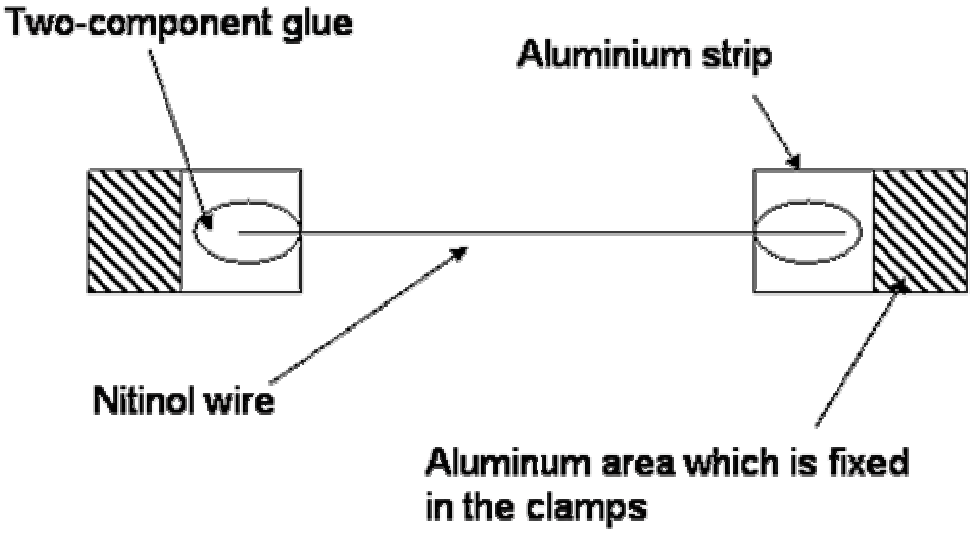

Fig.3.1: Schematical illustration of the Nitinol wire glued to an aluminium strip

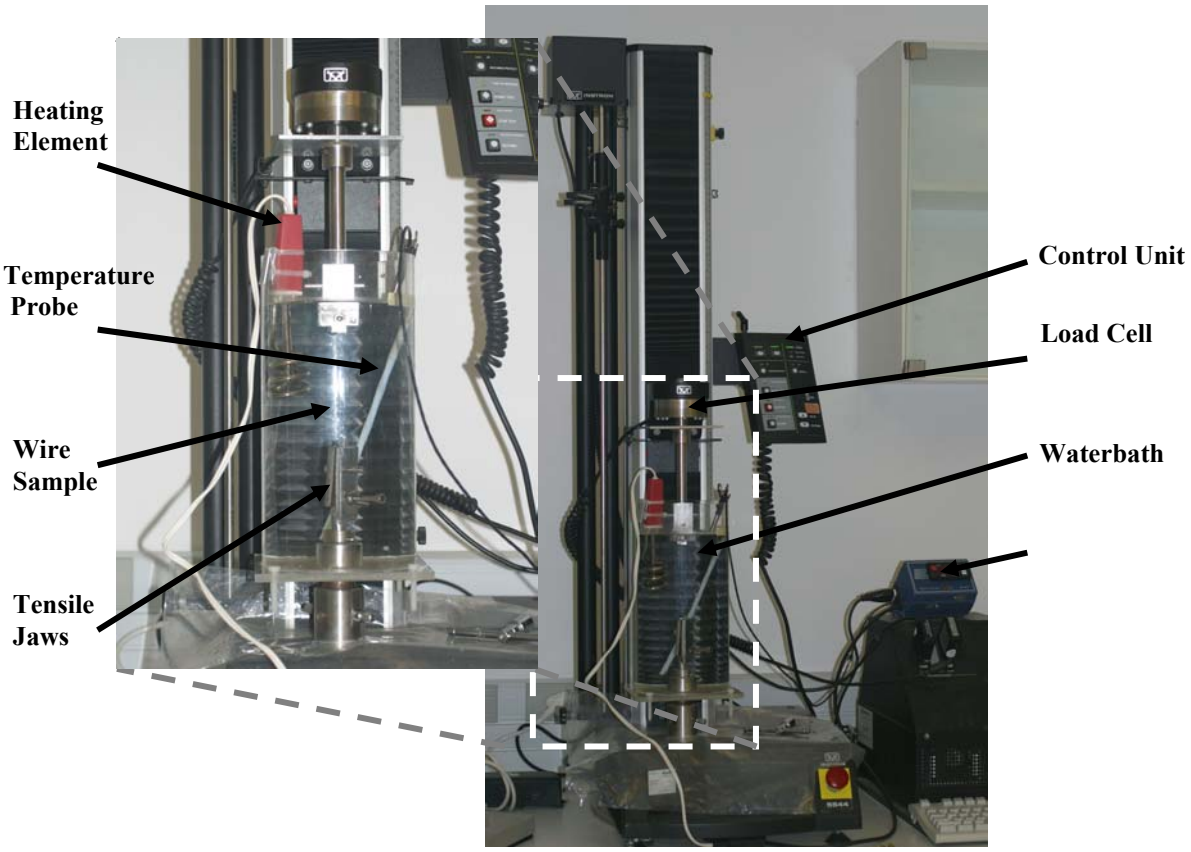

Fig.3.2: Tensile test machine from INSTRON with water bath for performing a wire tensile test at physiological body temperature

2.1.3 Constitutive equation

In the following the constitutive equations, after DIN EN 10 002 [17], for determination of strength and deformation parameters of a tensile test, are listed.

The normal stress σ of the wire is defined as

$$\sigma = \frac{F}{A_0}. \tag{3.1}$$

The force F is detected by the tensile machine and depends on the length variation of the wire

$$\Delta L = L - L_0. \tag{3.2}$$

The strain ε in [%] is given by

$$\varepsilon = \frac{\Delta L}{L_0} * 100\%. \tag{3.3}$$

Ultimate tensile strength is defined as

$$R_m = \frac{F_{\max}}{A_0} \tag{3.4}$$

The Young modulus is given by

$$E = \frac{\Delta\sigma}{\Delta\varepsilon} = \frac{F * L_0}{A_0 * \Delta L} \tag{3.5}$$

3.1.4 Program adjustment

The testing load was defined so that the superelasticity effect can be observed and that the deformations of the first three cycles are totally recovery. Cyclic tests were performed at 37° body temperature. Up to 3 1/2 cycles for each test were performed. The first 3 cycles were with a maximum load of 1.2 -1.4 N. In the last ½ cycle the wire was extended until it broke (see Fig. 3.3)

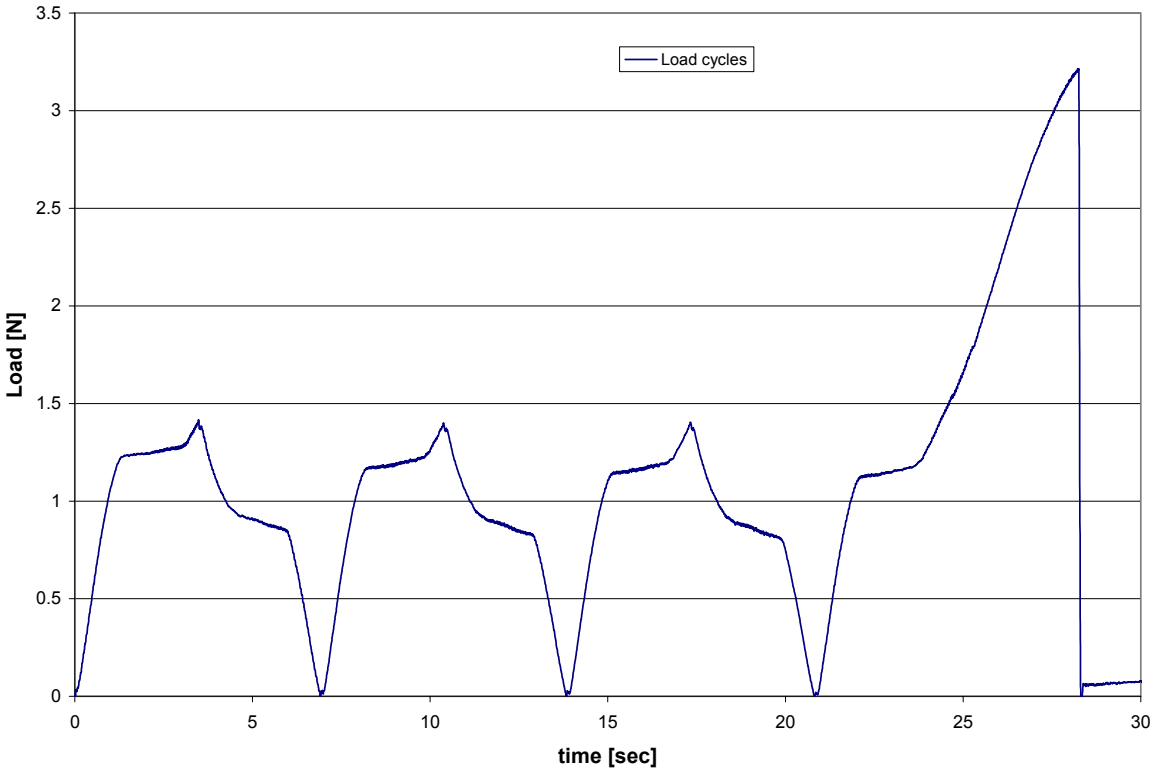

Fig.3.3: Example of the applied load for the wire tensile test over the time: 3 cycles at a certain load, ½ cycle for breaking the wire

The testing strain rate was adapted to the strain rate of load conditions for a Nitinol stent wire in the human body. Following calculation has been done to determine the strain rate of one cycle:

The average heart rate of a human body is:

$$Heartrate = 72\frac{beats}{\min} = 1.2\frac{beats}{\sec} \Rightarrow T = \frac{1}{1.2\frac{beats}{\sec}} \approx 0.83\sec \tag{3.6}$$

In one cardiac cycle, the systole last approximate 0.3 of the time period T. This means the strain load on the stent will be applied over $t_{sys} = 0.25\sec$ in one heart beat. By using the compliance equation [5]

$$C_d = \frac{d_{sys} - d_{dia}}{d_{dia}} \times \frac{100}{P_{sys} - P_{dia}} \times 100 \tag{3.7}$$

with $d_{dia} = 3.4mm$, $C_d = \frac{10\%}{100mmHg}$ and $\Delta P = 40$, the diameter variation of $\Delta d = 0{,}136mm$ is calculated. Thus, the perimeter variation is calculated as

$$\Delta P_{er} = 2\pi \frac{\Delta d}{2} = 0{,}42725mm . \tag{3.8}$$

The speed of one cycle is defined as

$$v = \frac{\Delta P_{er}}{t_{sys}} = \frac{0{,}42725mm}{0{,}25\,\text{sec}} = 1{,}709\frac{mm}{\text{sec}} = 102{,}54\frac{mm}{\text{min}} \tag{3.9}$$

Depending on the length of the wire and the crosshead speed of the clamps, the tested strain rates are calculated for sample lengths of $l_1 = 100mm$ and $l_2 = 40mm$ based on equations 3.10 and 3.11. Table 3.1 gives an overview of the testing strain rate values.

$$\varepsilon = \frac{\Delta l}{l} \tag{3.10}$$

$$\dot{\varepsilon} = \frac{\varepsilon}{t} \tag{3.11}$$

Table.3.1 Overview of test strain rates related on sample length and crosshead speed

sample length [mm]	crosshead speed [mm/min]	strain rate [1/sec-1]
40	2	3.30E-06
100	2	8.30E-04
40	102,54	0.067
100	102,54	0.017

Further setting or calculated values can be seen in Table A.1 in Appendix A.

3.1.5 Analysis of the data

The raw data which was captured by the computer, which is connected with the INSTRON tensile test machine, were analysed and prepare for use in determination the characteristic parameters of the Nitinol wire. Excel program was used as tool for the post-processing procedure. The comparative stress-strain curves for different SMA wires structure, an overview of obtained parameters and experimental data vs. FEM model data can be seen in the results chapter 4.1.1.

3.2 Finite Element Analyses

This section describes the development and settings of the following three FE models which were analysed in this work:

- SMA wire tensile test
- Helical Nitinol reinforcement model with Latex liner
- Braided stent model with Latex liner

Certain information about ADINA's capabilities and setting's options concerning the three models are presented:

- **Specifying Analysis Control Parameters:**

  In a model with only 3-D solid elements, all the rotational degrees of freedom should be fixed.

- **Defining Geometry:**

  There are three ways of creating the geometry for the ADINA analysis:

  - Developing the geometry in Pro/Engineer Wildfire. The Pro/Engineer geometry is converted to ADINA-Modeller as parasolid geometry via the interface between the both software programs. The parasolid geometry is then imported into ADINA-AUI for finite element modelling.
  - Developing geometry in Pro/Engineer Wildfire. The Pro/Engineer geometry is then converted into IGES format to import it into ADINA-AUI. The geometry is then imported as ADINA-M geometry with sheet bodies which have to be sewed before continuing with finite element modelling.
  - Developing geometry in ADINA-Modeller. ADINA-Modeller geometry consists of bodies, faces, and edges. The solid bodies, pipe and cylinder, which have been used in this work, are created from ADINA-M primitives (see Figure 3.4).

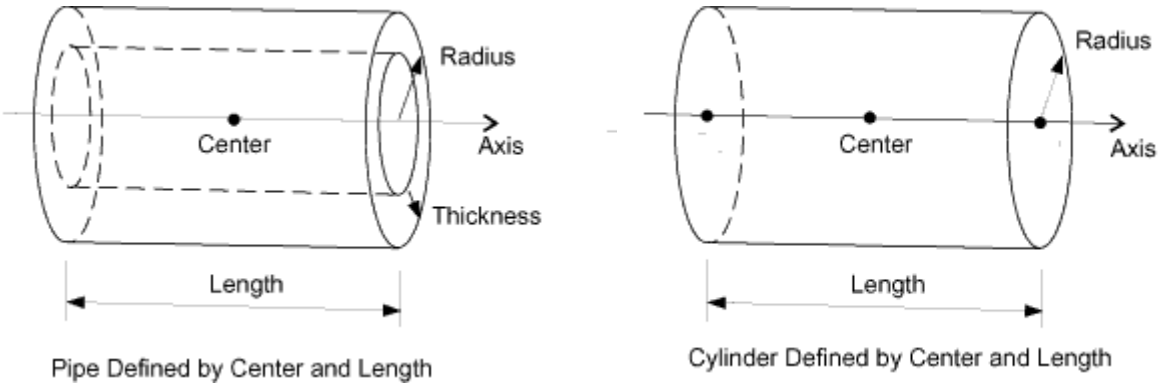

Fig.3.4: ADINA-M primitives' option to create pipe and cylinder geometries for the FE analysis [16]

- **Defining element type:**

  The Ogden material model, the SMA user supplied material and the fluid material model require 2-D or 3-D solid elements [16].

- **Mesh Generation:**

  In general, free-form meshing is used for bodies. Figure 3.5 presents available 3-D element types:

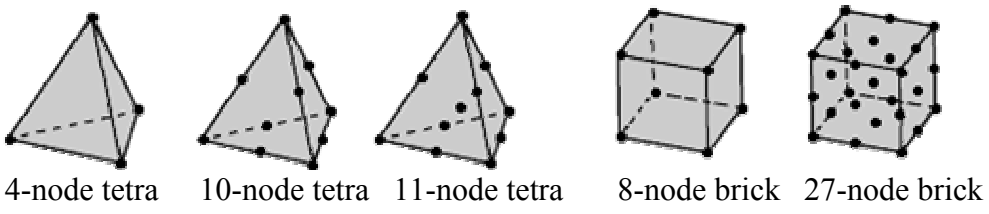

Fig.3.5: Available types of 3-D solid elements for free meshing of bodies

Concerning the available computer memory (2GB), the choice of the 3-D element type was limited. In the following sections "Definition of FEA model" of each FE model, the selected element type is described.

3.2.1 SMA wire tensile test

3.2.1.1 Problem description

A tensile test of Nitinol wires which are used for the production of the stent structure was analysed (see Fig.3.6). The user-subroutine material model for SMA from Meissner [9] was used.

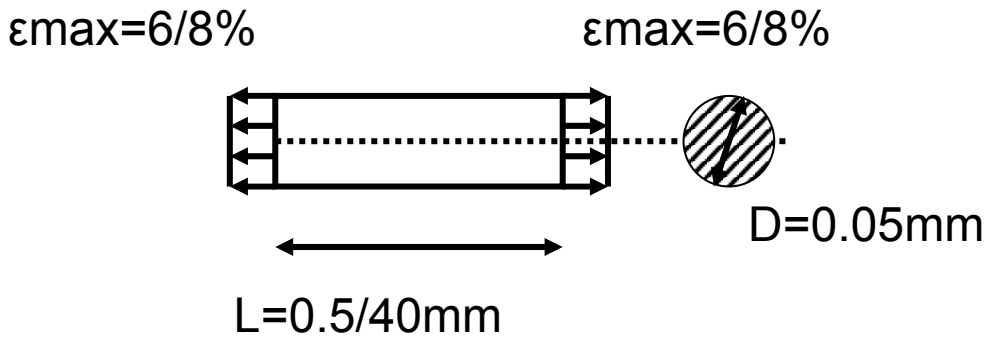

Fig.3.6: Geometry of the tensile test FE wire model

3.2.1.2 Definition of FEA model

Six different FEM wire tensile test analysis were performed and compared to the experimental data. Three tests were performed with the Nitinol wire (ARM0102) mechanical properties set from Table 4.2 (see result chapter 4) and three tests were performed with the Nitinol wire mechanical properties set from Table 4.2 for the ARM0103 Nitinol wire. 3-D 4-nodes or 8-nodes solid elements were used to model the cylinder. The length of the simulated wire was 0.5 or 40 mm. The parameters of the six tensile tests are shown in Table 3.2.

Tab.3.2: Overview of simulated wire and parameters of the FEM tensile tests

Wiretyp	max strain [%]	element family	element type	length of wire [mm]
Nitinol ARM0102	6	3-D solid	4-nodes tetrahedral	0.5
Nitinol ARM0102	6	3-D solid	8-nodes brick	0.5
Nitinol ARM0102	6	3-D solid	8-nodes brick	40
Nitinol ARM0103	8	3-D solid	4-nodes tetrahedral	0.5
Nitinol ARM0103	8	3-D solid	8-nodes brick	0.5
Nitinol ARM0103	8	3-D solid	8-nodes brick	40

The material properties for both wires which were required for using the SMA user subroutine material model are assumed as in Table 4.1. At one end of the wires a displacement was

prescribed as a linear external load so that the wire has the same maximum strain and strain rate like in experimental test. The linear displacement history is illustrated in Figure 3.7. To obtain a superelastic reaction of the wires and to guarantee the same temperature condition like in the body, the temperature was fixed at T=37°C at the model nodes. Using uni-axial load, wire tensile test was analysed and compared to experimental data see result section in chapter 4.

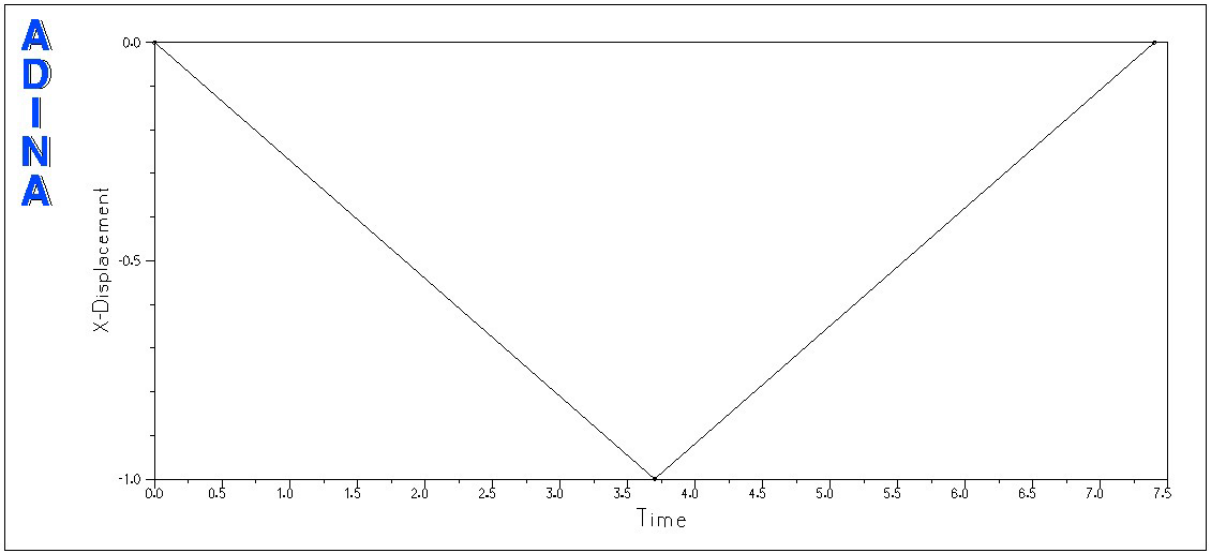

Fig.3.7: Displacement loading: one load cycle takes 7.3 sec

3.2.2 Helical Nitinol reinforcement model with Latex liner

3.2.2.1 Problem description

In the arteries, the cyclical difference between systolic and diastolic pressures generates the most significant forces on cardiovascular prostheses. A 3-D geometrical model was developed to analyse the stresses and strains caused by the physiological loading condition of the cardiovascular prostheses. A latex liner, which is commonly used for in vitro compliance tests, was developed. The fluid directly interacted with the latex liner and the prosthesis structures will be loaded using contact mechanisms. Therefore, the radial geometrical dimensions of the components were matched to each other so that the mechanisms were realised (see Figure 3.8). The longitudinal length was defined regarding that the required memory doesn't rise above the computer limit.

In this problem the following steps were performed:

- Defining the Latex-material model
- Developing of the Geometry of the Latex tube
- Developing and importing the helical reinforcement structure from Pro/Engineer Wildfire to ADINA.
- Defining the SMA user material model for helical reinforcement
- Defining the contact behaviour between helical reinforcement structure and Latex liner
- Defining the 3-D fluid model
- Defining the Fluid-Structure-Interaction (FSI)

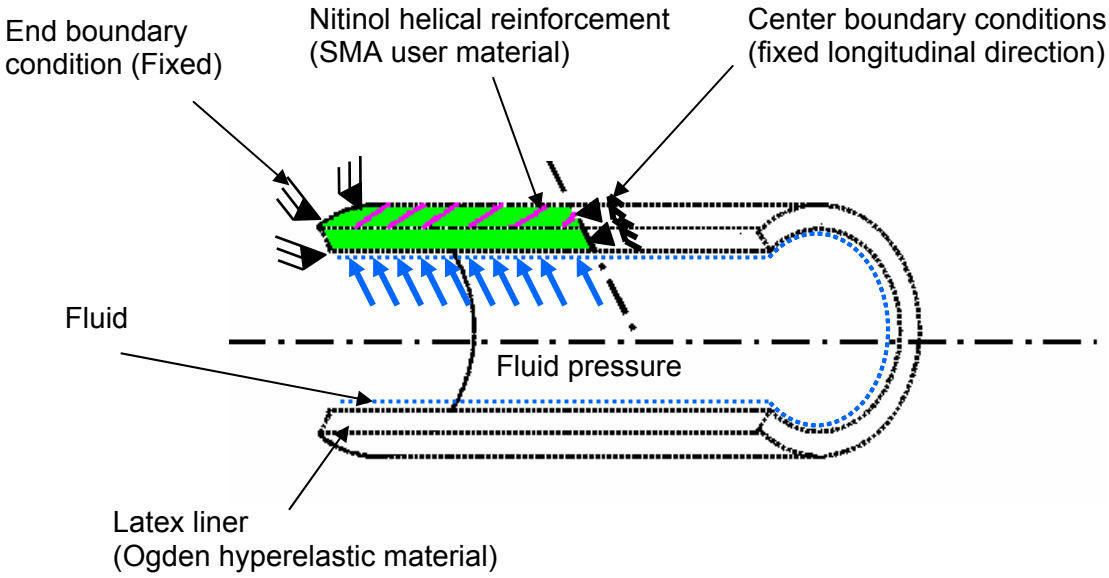

Fig.3.8: FE model illustration of helical reinforcement Nitinol model with latex liner and fluid

3.2.2.2 Definition of FEA model

Fluid model

A 3-D geometry model was developed with ADINA. 3-D 4-nodes tetrahedral fluid elements were used to model the fluid cylinder. The length of the fluid model was 3mm. The model radius was 1.2246mm. The fluid interacted mechanically with the latex tube. The model was simplified concerning the simulation of blood fluid flow. The following assumptions have been done:

- The fluid was homogenous and Newtonian
- The fluid was incompressible and the fluid flow laminar

- The fluid properties were constant over time:

Viscosity: $\mu = 10^{-9} \frac{\text{Nsec}}{\text{mm}^2}$

Density: $\rho = 8.9 \times 10^{-10} \frac{\text{Nsec}^2}{\text{mm}^4}$

Fluid bulk modulus: $K = 2000 \frac{\text{N}}{\text{mm}^2}$

Latex model

A 3-D Latex geometry model was developed with ADINA. 3-D 4-nodes tetrahedral solid elements were used to model the Latex tubular structure. The dimensions of the geometry model adapted to the prostheses dimensions were:

Length: $l = 3\text{mm}$

Radius: $r = 1.395\text{mm}$

Thickness: $t = 0.25\text{mm}$

The ADINA Ogden material model was used to describe the mechanical properties of the Latex Liner. Experimental strain-stress values received form Latex material tests under pressure loading condition approximating the blood pressure of a cardiac cycle (described in [5]) were used to define the Ogden material constants and bulk modulus. In [5], FE tensile tests (ABAQUS) with defined Latex material model have been performed and the results compared to experimental data. The comparative curves for the latex experimental data vs. the numerical results of Latex material model are shown in Figure 3.9. The data demonstrates that the numerical solution fits and follows the experimental data.

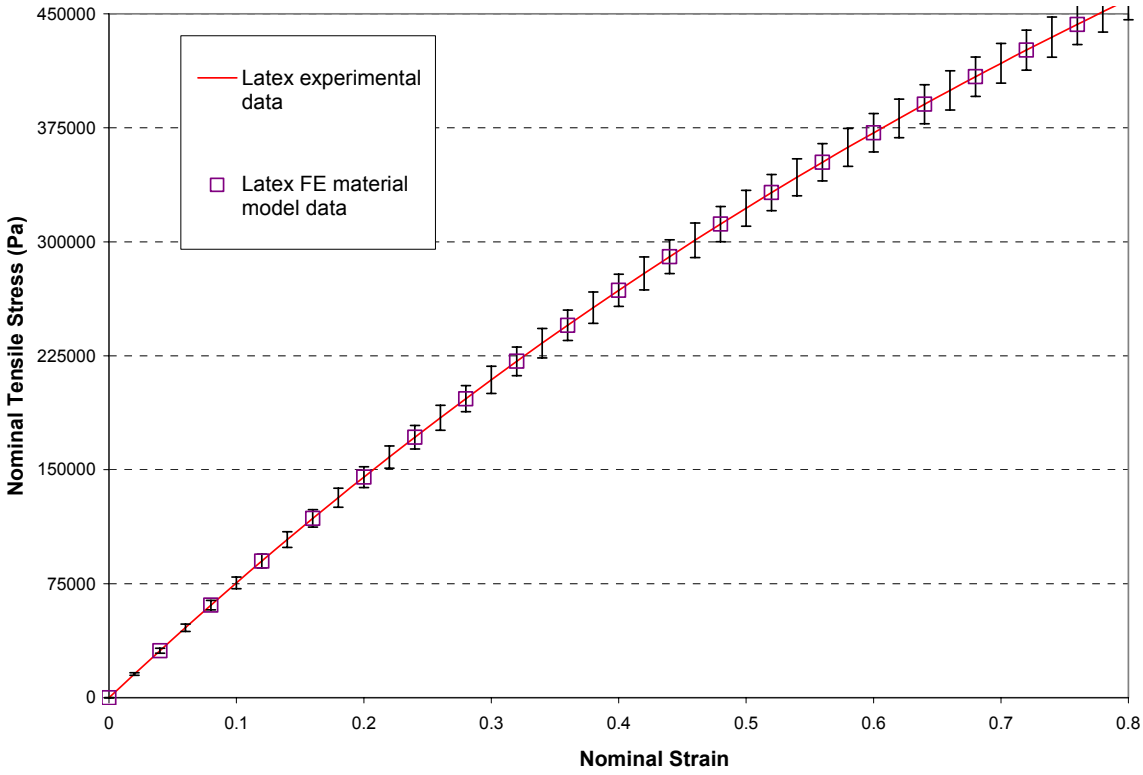

Fig 3.9 Comparative curves for the latex experimental data vs. the numerical results of Latex material model

With the assumption that, the computational model data for strain and stress utilised in ADINA have similar results to the results in Figure 3.8, the data were used in this work. ADINA performed a curve fit with the strain-stress input data to determine the hyperelastic material constants for the Ogden material model. The order of the approximation was set to n=6. The Bulk Modulus K and the Ogden material constants, μ_n and α_n, were calculated. Figure 3.10 displays the stress-strain curve.

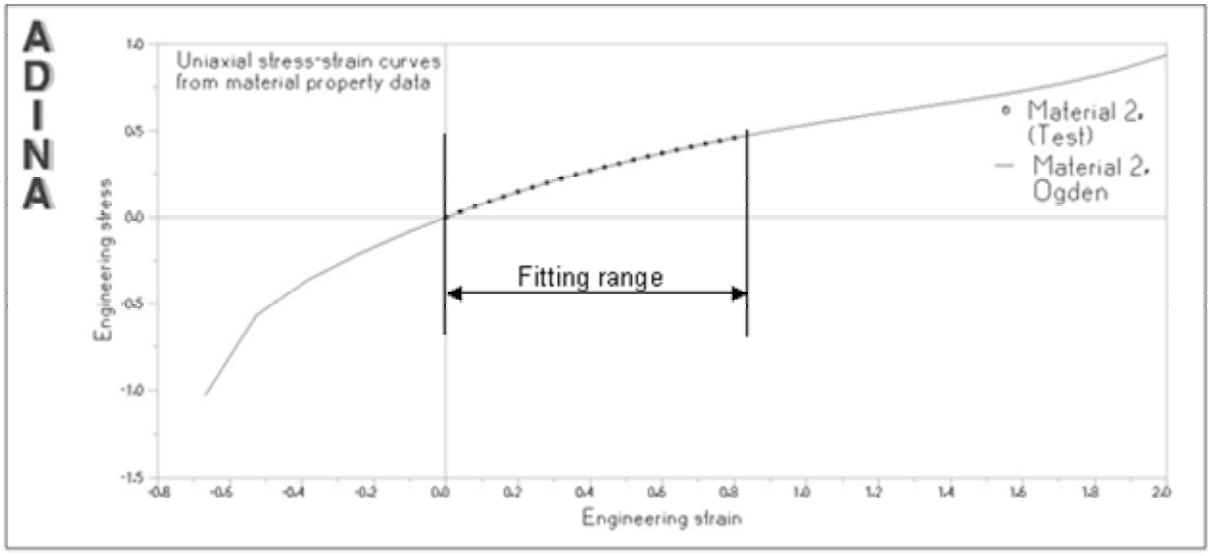

Fig 3.10 Latex stress-strain curve: ADINA performs a curve fit to determine the hyperelastic material constants for the Ogden material. The fitting range is limited between 0-0.8% strain. The magnitude of strain values results of the Latex structure fits in this range.

The Latex liner was fixed at one end in all direction. Centre boundary conditions were applied to define symmetry conditions: the longitudinal direction was fixed, the other degree of freedom were free.

Helical reinforcement model

A 3-D helical reinforcement geometry model was developed in Pro/Engineer Wildfire (see Fig.3.11). The dimensions of the geometry model were:

Length: $l = 3\text{mm}$

Radius: $r = 1.645\text{mm}$

Wire thickness: $t = 0.05\text{mm}$

Pitch: $p = 50$

3-D 4-nodes tetrahedral solid elements were used to model the helical reinforcement structure in ADINA. The SMA user material model was used for the Nitinol helical reinforcement structure. The material properties from the Nitinol wire ARM0102, as described in chapter 4.1.2, were used to define the mechanical properties of the structure.

To obtain a superelastic behaviour of the helical reinforcement and to guarantee the same temperature condition like in the body, the temperature was fixed at T=37°C for the entire loading time period at the model nodes.

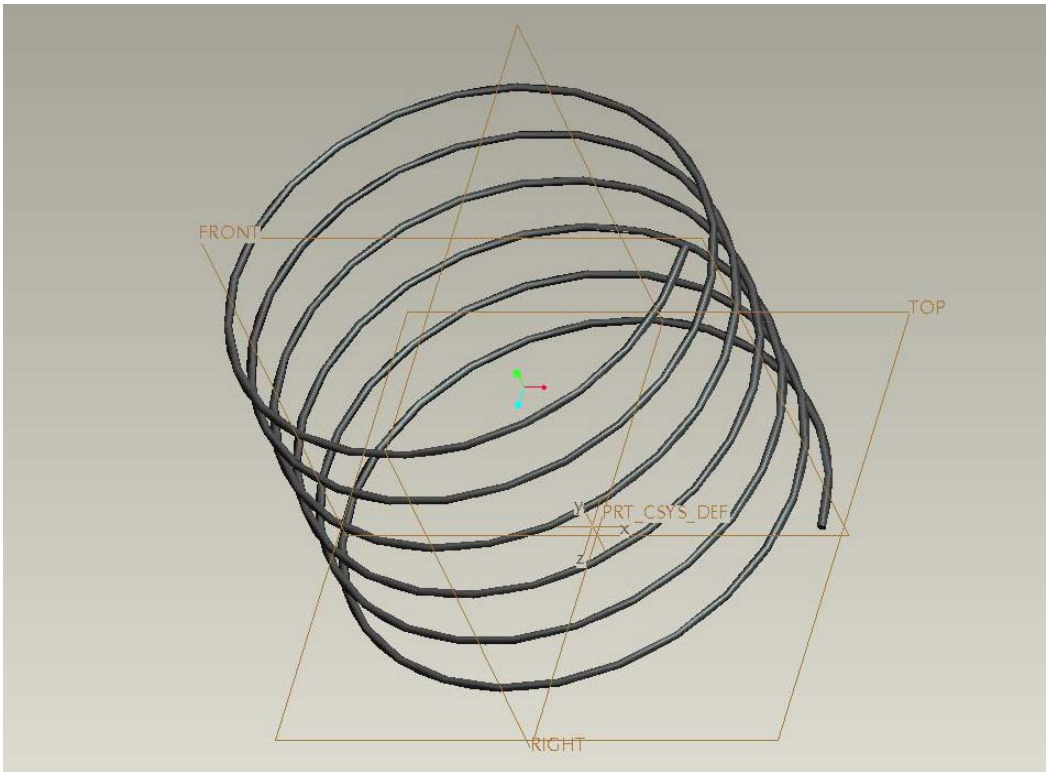

Fig.3.11: 3-D helical reinforcement geometry model developed in Pro/Engineer Wildfire

Interface of Latex and helical reinforcement structure:

At the interface of the Latex pipe and the helical reinforcement structure, a segment contact mechanism is applied. The basic steps to prepare a model for contact analysis are as follows:

- Define contact surfaces
- Define contact pairs

To stabilize the contact problem master/slaves constrains were defined. As the nodes displace due to deformation, the slave node is constrained to translate and rotate such that the distance between the master node and the slave node remains constant and that the rotations at the slave node are the same as the corresponding rotations at the master node.

Fluid-Structure interaction

Special FSI-boundary conditions, fluid structure interaction between the contact surfaces of each component, were applied on the cylinder surface of the fluid model and on the tube inner surfaces of the Latex liner. Additionally, at the interface of the fluid and the Latex inner surface, slip conditions were applied. The fluid velocity vector on that wall was prescribed not to

be zero, $v_{fluid} \neq 0$. A fixed wall condition was applied at the end of the model where the Latex structure is fixed. There, the boundary displacement of the fluid is zero.

Loading condition

The loading condition for this analysis simulates the mechanical loading of the artery wall at one cardiac cycle. Therefore, a transient radial pressure was applied on the fluid model. The pressure was defined as "normal traction" over a period of 0.83 sec. The load was applied in 100 times steps. The transient pressure curve is illustrated in Fig.3.12.

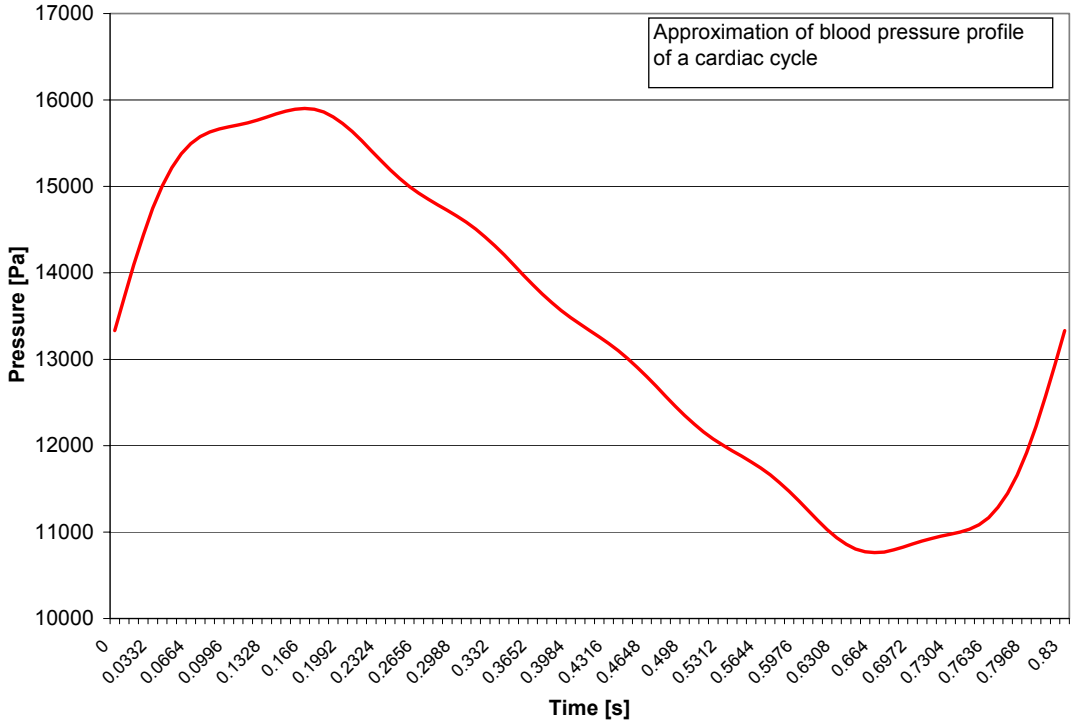

Fig.3.12: Applied loading condition: Approximated pressure curve simulate the loading condition of one cardiac cycle

3.2.3 Braided stent model with Latex Liner

3.2.3.1 Problem description

A second 3-D geometrical model was developed to analyse the stresses and strains caused by the physiological loading condition of cardiovascular prostheses (see Figure 3.13). The problem was similar to the "helical Nitinol reinforcement model with Latex liner" problem with the difference that a braided Nitinol structure served as component of cardiovascular prostheses instead of the helical reinforcement. A stent is a metal mesh made from fine wires with desired design. To avoid repeating the problem description of the "helical Nitinol reinforcement model with Latex liner" problem, only the differences to the previous model are presented.

In this problem the following additional steps was required:

- Importing the braided stent structure from Pro/Engineer Wildfire to ADINA and defining SMA user material model.

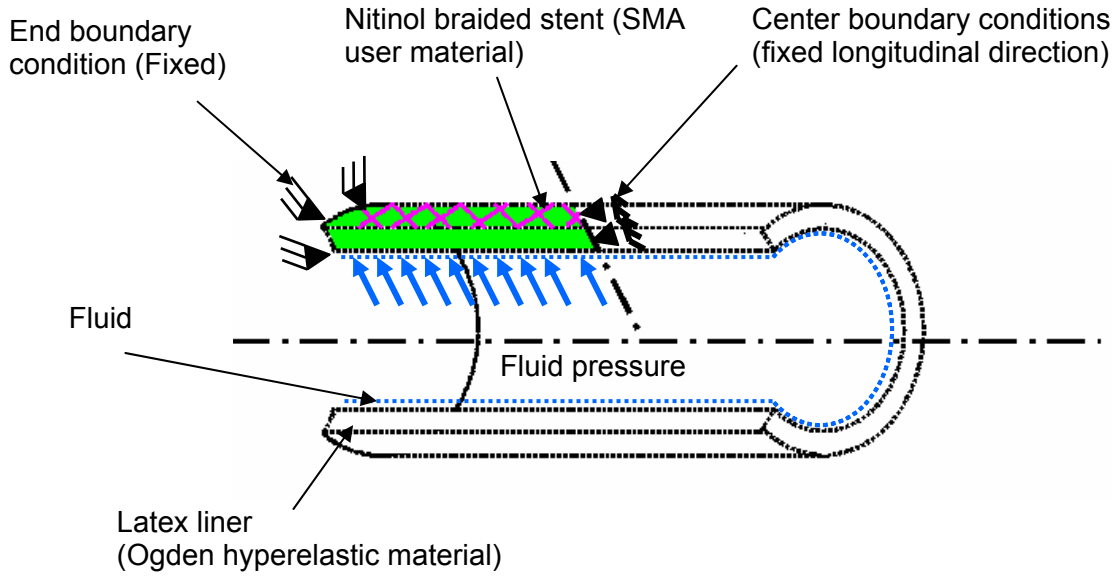

Fig.3.13: FE model illustration of Nitinol braided stent model with latex liner and fluid

3.2.3.2 Definition of FEA model

To avoid repeating the definition of the "helical reinforcement Nitinol model with Latex Liner" model, the particular parts are summarized and the difference presented. The development the components of the braided stent model followed the same procedure as described for the helical reinforcement Nitinol model

Fluid model

A 3-D geometry model was developed with ADINA. 3-D 4-nodes tetrahedral fluid elements were used to model the fluid cylinder. The geometry dimension, length =3mm and radius =1.2246mm, were chosen as in the helical reinforcement Nitinol model. The fluid interacted mechanically with the latex tube. The model was simplified and the fluid was assumed to be homogenous, Newtonian, incompressible and laminar fluid flow. The fluid properties were defined as in the helical reinforcement Nitinol model :

Viscosity: $\mu = 10^{-9} \frac{\text{Nsec}}{\text{mm}^2}$

Density: $\rho = 8.9 \times 10^{-10} \frac{\text{Nsec}^2}{\text{mm}^4}$

Fluid bulk modulus: $K = 2000 \frac{\text{N}}{\text{mm}^2}$

Latex model

A 3-D Latex geometry model was developed with ADINA. 3-D 4-nodes tetrahedral solid elements were used to model the Latex tubular structure. The dimensions of the geometry model were defines as in the helical reinforcement Nitinol model:

Length: $l = 3\text{mm}$

Radius: $r = 1.395\text{mm}$

Thickness: $t = 0.25\text{mm}$

The ADINA Ogden material model was used to describe the mechanical properties of the Latex Liner. Experimental strain-stress values received form [5] were used to define the Ogden material constants and bulk modulus by curve fitting as it was described in helical reinforce-

ment Nitinol model. The order of the approximation was set to n=6. The Bulk Modulus K and the Ogden material constants, μ_n and α_n, were calculated.

The Latex liner was fixed at one end in all direction. Centre boundary conditions were applied to define symmetry conditions: the longitudinal directions were fixed, the other degree of freedom were free.

Braided stent model

A 3-D braided stent geometry model was developed in Pro/Engineer Wildfire (see Fig.3.14). The dimensions of the geometry model, length: $l = 3\text{mm}$, radius: $r = 1.645\text{mm}$,wire thickness: $t = 0.05\text{mm}$ and pitch: $p = 50$ were defined as in the helical reinforcement model.

The Pro/Engineer braided stent geometry was converted into IGES format to import it into ADINA-AUI. The geometry is then imported as ADINA-M geometry with thee sheet bodies option which have to be sewed before continuing with finite element modelling.

3-D 4-nodes tetrahedral solid elements were used to model structure in ADINA. The material properties from the Nitinol wire ARM0102 were used to define the mechanical properties of the SMA user material model.

The temperature was fixed at T=37°C for the entire loading time period at the model nodes.

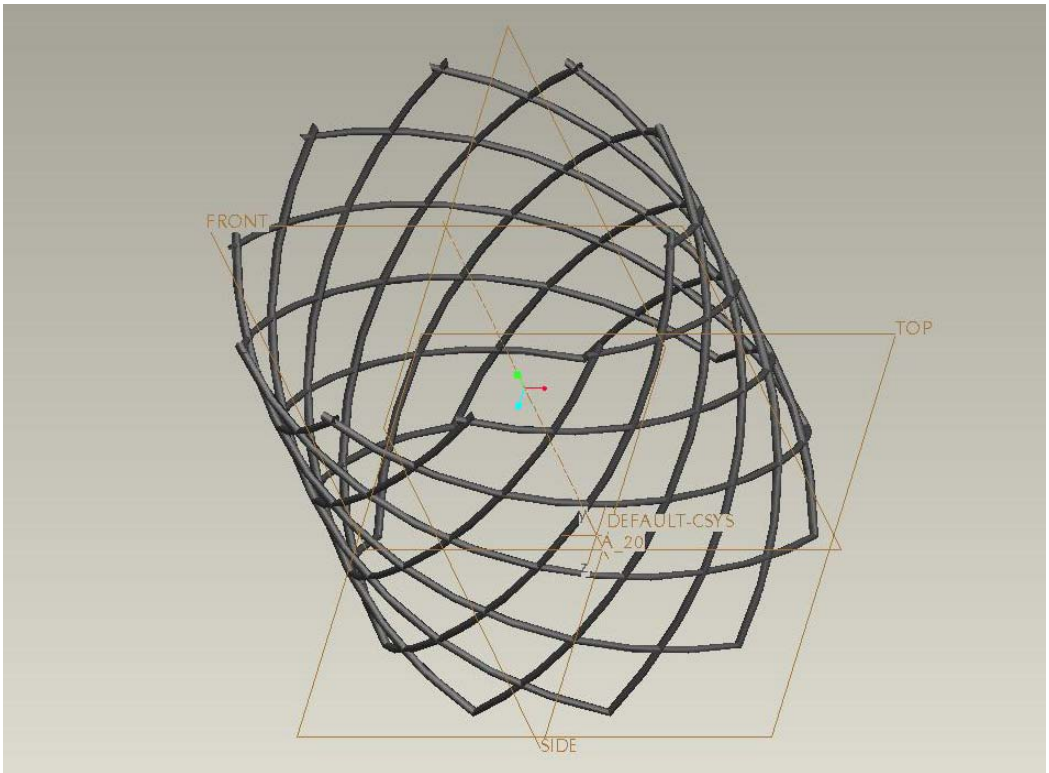

Fig.3.14: 3-D Nitinol braided stent geometry model developed in Pro/Engineer Wildfire

Interface of Latex and helical reinforcement structure:

At the interface of the Latex pipe and the helical reinforcement structure, a segment contact mechanism is applied. To stabilize the contact problem master/slaves constrains were defined.

Fluid-Structure interaction

Special FSI-boundary conditions were applied on the cylinder surface of the fluid model and on the tube inner surfaces of the Latex liner. Additionally, at the interface of the fluid and the Latex inner surface, slip conditions were applied. A fixed wall condition was applied at the end of the model where the Latex structure is fixed. There, the boundary displacement of the fluid is zero.

Loading condition

The loading condition for this analysis was defined as in the helical reinforcement model. A transient radial pressure was applied on the fluid model. The pressure was defined as “normal traction” over a period of 0.83 sec. The load was applied in 100 times steps.

4 Results

This chapter describes the results of the finite element analysis of three models: the SMA wire tensile test, the helical reinforcement Nitinol model with Latex Liner and the braided stent model with Latex Liner. The simulations were carried out with following material models which have been proved accurate before: Fluid, hyperelastic rubber material (Latex) and Shape Memory Alloy (Nitinol). The results of an experimental tensile test for Nitinol wires are presented. During the development of the geometrical and material models, different simplified simulation models were investigated to establish the ideal parameters setting for the final models. The results of the three final simulation models and of the experiments are shown and discussed in this chapter.

4.1 SMA wire tensile test

4.1.1 Experimental SMA wire tensile test

For the usage of the FEM SMA material model from Meissner [9] a list of input values (see chapter 2.4.1.2) has to be defined. Thus, parameter value identification has to be carried out. Additionally, the FEM material model needs to be validated against experimental data to confirm that the SMA material model can be used with confidence for further simulation. Therefore, uni-axial experimental wire tensile tests were carried out. Chapter 3.1 presents the protocol for experimental SMA wire tensile test with relevant information about the experiment set-up, constitutive equations and boundary condition.

From the analysis of the experimental tensile test data, the mechanical properties of different Nitinol wires were determined. Young's modulus, stress-induced transformation stresses and strains, ultimate tensile stress and strain to failure are shown in Tab 4.1. The table is a comparison of the values for the 3rd unloading and 4th loading cycle of each test.

Tab.4.1: Comparison of mechanical properties of the tested wires from the experimental wire tensile test

Experimental Wire tensile test- results																	
Wire	experiment #	E_A [MPa]	E_M [MPA]	σ_up [MPa]	σ_low [MPa]	uts [MPa]	ε_max [%]	ε_p [%]	ε_Af [%]	ε_As [%]	ε_Ms [%]	ε_Mf [%]	σup_Ms [MPa]	σup_Mf [MPa]	σdown_Af [MPa]	σdown_As [MPa]
ARM0137	3	135740				1629.822	1.606039									
ARM0137	4-7	137460														
ARM0137	8-11	164780														
Lot #035906	21-24	49744														
Lot #035906	25-26	53208														
Lot #035906	27	53287														
ARM0103	29-32	20698														
ARM0103	33-36	20201		500	295				1.8	6,4	2.5	7.7	441	611	85	374
ARM0103	37	20373		437	250				0.5	3.12	1.4	3.8	426	611	31	322
ARM0103	38		11296	382		1247.951	13.51716				2.5	6.5	381	428		
ARM0002	39	25240														
ARM0002	44	24316		531	337				0.6	5.8	2.4	7.2	496	661	100	396
ARM0002	45	25898		531	337				0.5	2.4	21	7.3	491	659	63	385
ARM0002	47	24509	21683	492	290	1412.85	11.59019		0.5	6	2	7	430	668	100	358
ARM0102	1	33058														
ARM0102	2	33093	12489	615	485			0.042708	1	5	2	5	561	709	300	565
ARM0102	3	31700	16183	590	470	1696.808	13.01935	-0.00875	1	4.8	2.1	5	553	724	300	552
ARM0102	4	32400	16701	589	440	1637.892	12.75623	0.076458	0.9	5.2	1.9	6	530	722	236	535
ARM0102	5	36564	17192	620	472	1828.133	13.38102	0.09625	1	4.6	1.9	5.5	540	717	294	560
ARM0102	6	32527	15353	616	460	1586.657	11.95081	-1.052707	0.4	5	2	5.9	563	722	95	574
ARM0102	7	32005	15892	540	382	1651.843	13.79748	0.317291	0.5	5.4	1.9	6.6	479	723	67	512
ARM0102	8	32670	16710	573	432	1687.963	13.6331	0.203333	0.7	5.3	1.9	6.2	500	715	188	543
ARM0102	10	33399		598	440			0.112083	1	5	2	6	537	716	272	535

Typical tensile testing results are shown in Fig.4.1, where the different heat-set and non-heat-set Nitinol wire specimens are recorded. The data verified the superelastic behaviour of the heat-set Nitinol wires (ARM0002, ARM0103, ARM0102) compared to the linear behaviour of the non-heat-set wires (ARM0137, Lot# 035906) at 37 °C physiological body temperature. The stress-strain curves of the heat-set specimen have distinct stress plateaus (upper and lower) due to the phase transformation between martensite and austenite. Additionally, different Young's moduli for austenite and martensite can be observed depending on the wire type. Heat-set wires demonstrate lower Young moduli for austenite then non-heat-set wires.

To underline the significant difference between heat-set and non-heat-set Nitinol wires, tested at a strain rate of $\dot{\varepsilon} = 0.017 \frac{1}{\text{sec}}$, two curves are compared: ARM0137 and ARM0102 (see Fig.4.2). The ARM0102 wire shows SMA typical superelasticity behaviour. The ARM0137 wire deforms linear with increasing load and breaks at strain to failure. Therefore, the assumption is made that the ARM0137 wire is non-heat-set.

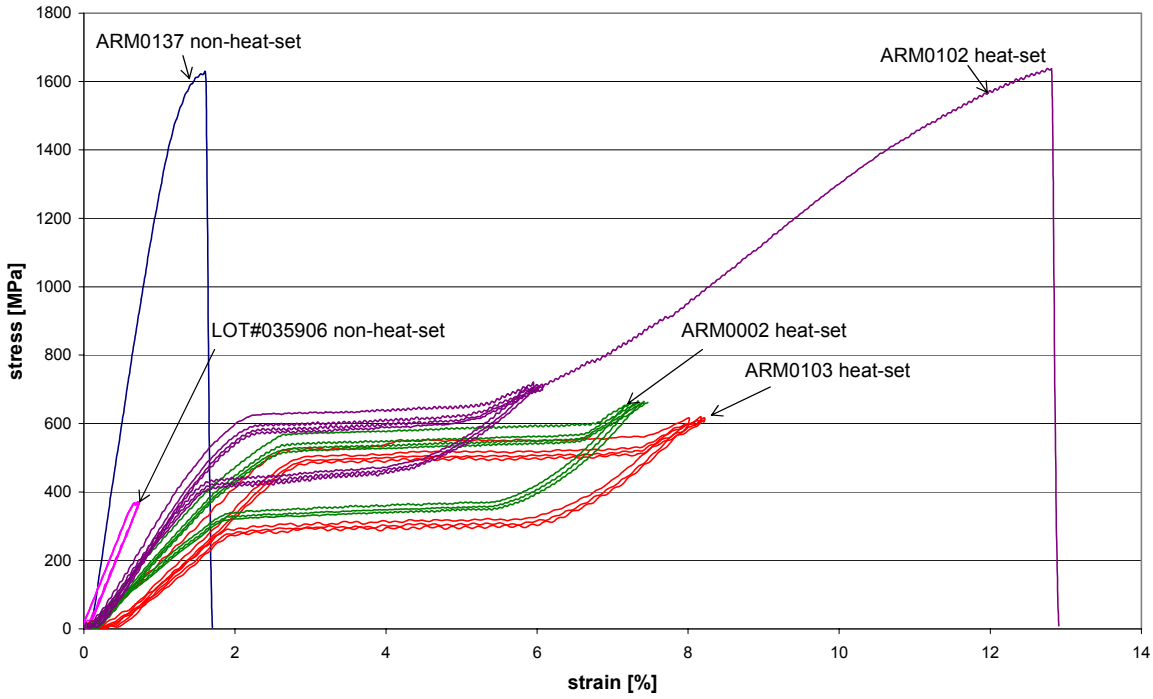

Fig.4.1: Comparison of stress-strain curves of heat-set and non-heat-set Nitinol wires under Tension at T=37°C

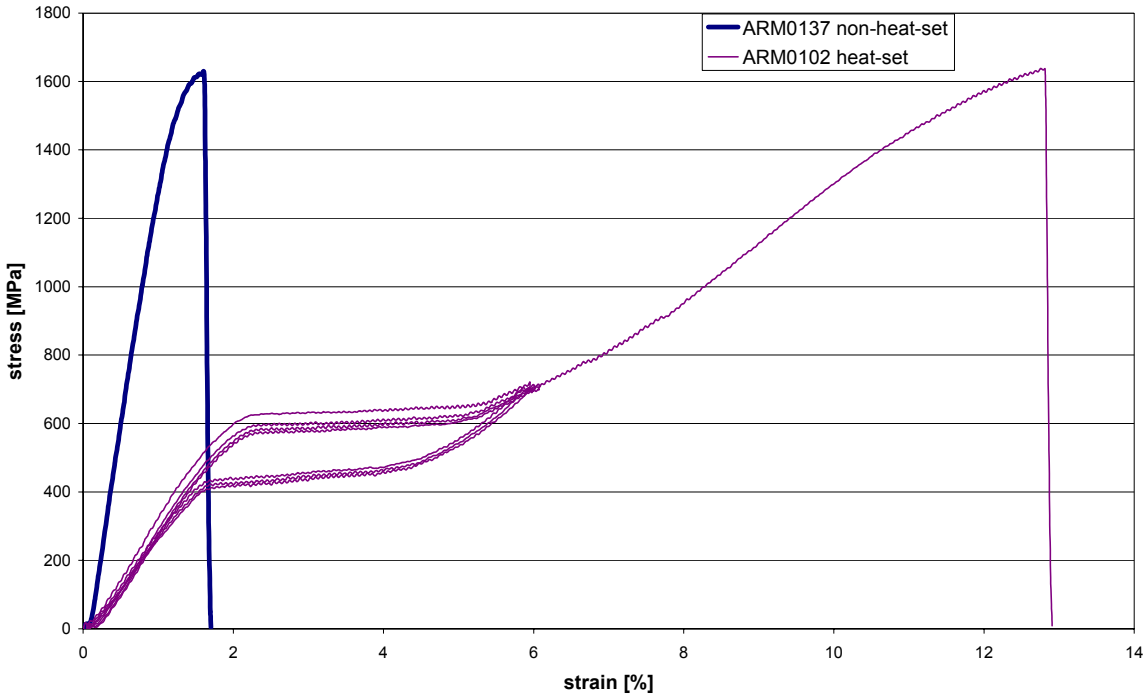

Fig.4.2: Comparison of two stress-strain curves of heat-set wire (ARM0102) and non-heat-set wire (ARM0137) at $T = 37°C$ and strain rate of $\dot{\varepsilon} = 0.017 \frac{1}{\text{sec}}$.

The stress-strain curves of the last 1.5 cycles of three ARM0102 samples at the high strain rate of $\dot{\varepsilon} = 0.017 \frac{1}{\text{sec}}$ are plotted in Fig.4.3. The conditions for the three cycles were the same. They represent a similar cyclic behaviour of the cycles.

Five characteristic regions can be identified and classified in the graph.

1. Region I shows the elastic deformation of Nitinol. The gradient of the strain-stress curve in this region is called Young's modulus of austenite.
2. Region II presents the pseudoelasticity (upper stress plateau). In this region, the transformation from austenite to martensite is taking place.
3. Region III starts from the end of the upper stress plateau and is related to the elastic deformation of martensite. With further increasing the load, plastic deformation of martensite will occur.
4. Region IV is classify as the region starting from end of the upper stress plateau and ends at the beginning of the lower stress plateau.
5. Region V presents the pseudoelasticity (lower stress plateau). The transformation from martensite to austenite is taking place.

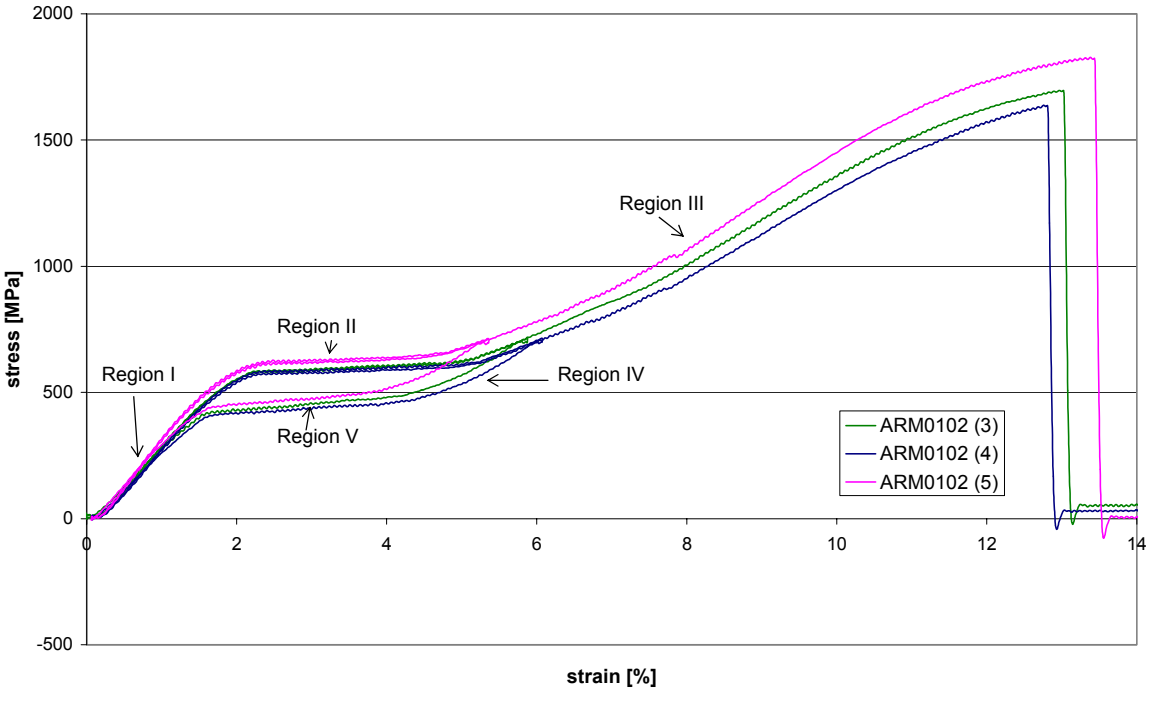

Fig.4.3: Similar cyclic behaviour of Nitinol wire at testing temperature of T=37°C and at the strain rate of $\dot{\varepsilon} = 0.017 \frac{1}{\text{sec}}$

Three wires were tested at the same temperature condition as the wires but at lower strain rate $\dot{\varepsilon} = 3.3\text{E-}4 \frac{1}{\text{sec}}$, to demonstrate the influence of the strain rate on the mechanical behav-

iour of the Nitinol wires. The stress-strain curves of the last 1.5 cycle of three ARM0102 wire at the low strain rate of $\dot{\varepsilon} = 3.3\text{E-}4 \frac{1}{\text{sec}}$ are plotted in Fig.4.4. They represent similar cyclic behaviour.

Figure 4.5 displays the curves results at low strain rate of $\dot{\varepsilon} = 3.3\text{E-}4 \frac{1}{\text{sec}}$, compared with the results of high strain rate of $\dot{\varepsilon} = 0.017 \frac{1}{\text{sec}}$. The Tab.4.1 underlines the results which can be determined from the graphs.

Following statements can be done:

- The ARM0102 wires tested at the high strain rate have higher Young's moduli of austenite then the same type of wire tested at the low strain rate.
- The stress-induced transformation stress plateaus (upper and lower) are dependent on the strain rate. At lower test strain rate the stress plateau values are lower than at high strain rate. Especially the lower stress plateaus at lower strain rate clearly differ from that at high strain rate.
- The ultimate tensile stress values of the wire tested at high strain rate are higher than those of the lower strain rate tests. The strains to failure of both wires lie in the range of 12-14%.

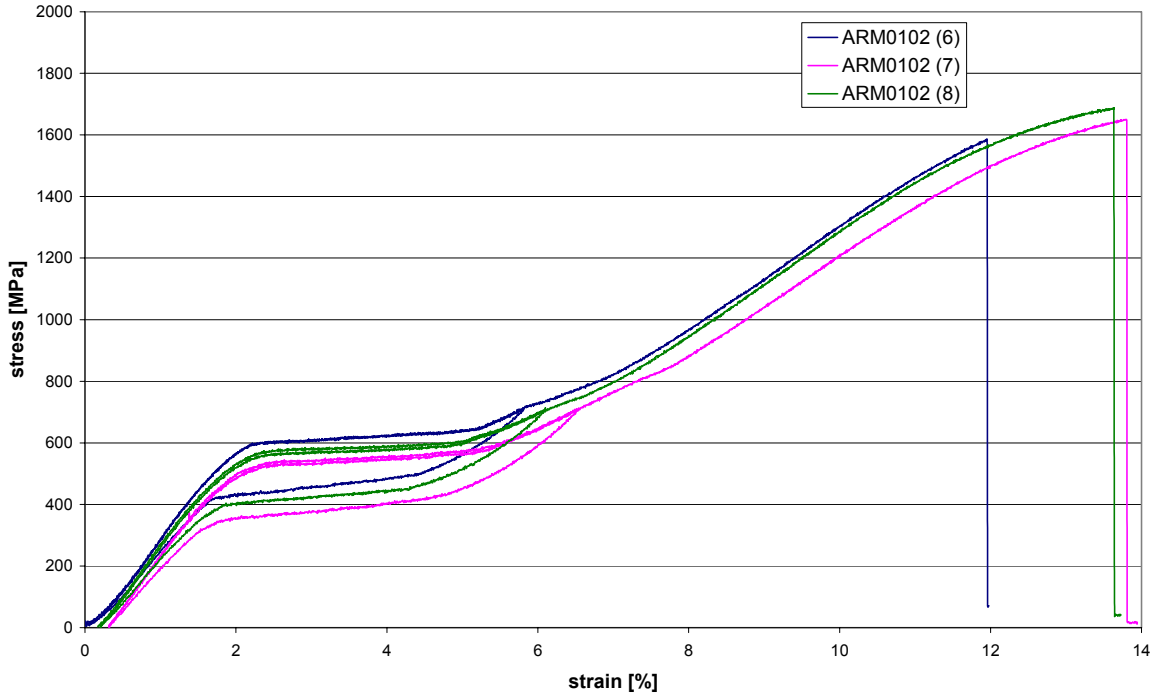

Fig.4.4: Three Nitinol wires (ARM0102) at the strain rate of $\dot{\varepsilon} = 3.3\text{E-}4 \frac{1}{\text{sec}}$

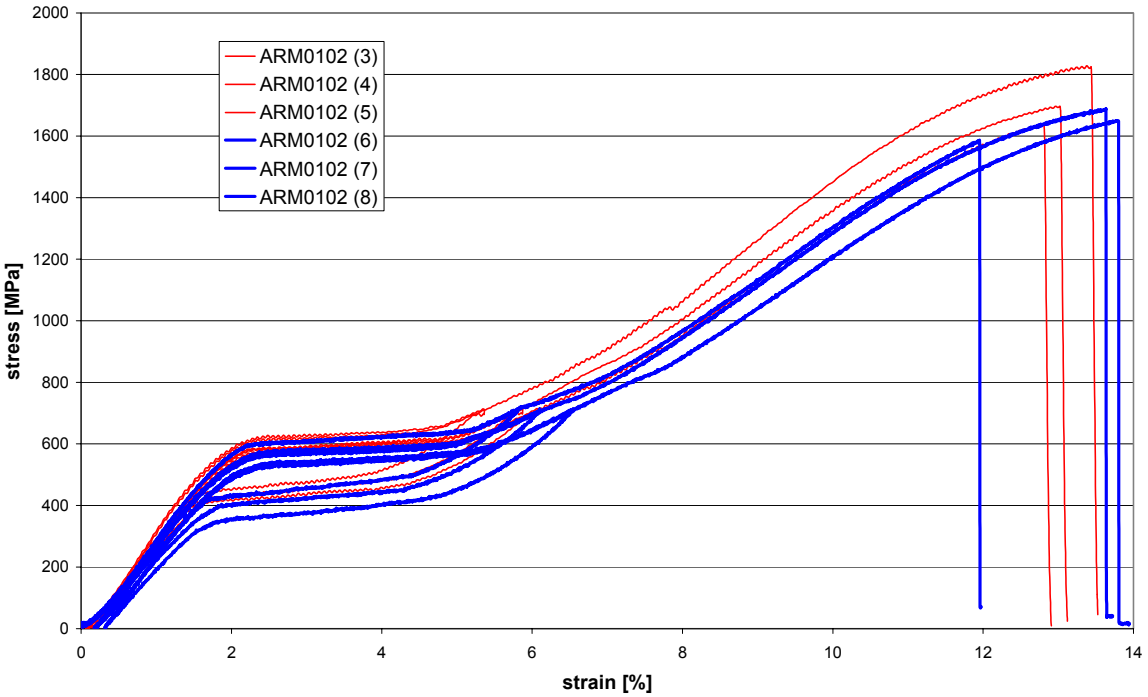

Fig.4.5: Three Nitinol wires (ARM0102) at the strain rate of $\dot{\varepsilon} = 3.3\text{E-}4\,\frac{1}{\text{sec}}$ (thin red lines) compared to three Nitinol wires (ARM0102) at the strain rate of $\dot{\varepsilon} = 0.017\,\frac{1}{\text{sec}}$ (thick blue line).

In addition, two screening tests were performed: One for the analyses of the temperature influence of Nitinol and one for proving the training behaviour of the Nitinol wire. For both tests ARM102 wires were used.

The tensile stress-strain curves of Nitinol for different temperature conditions (T=21, 10, 0°C), are shown in Fig. 4.6. For clarity, the last 1.5 cycles are shown on the graph. The results indicate that if the temperature is decreasing the stress-induced transformation stresses and strains will be decreasing. On the other hand, the ultimate tensile stress and strain to failure of the wires, tested at lower temperature than 37°C, are higher than those of the wires tested at 37°C.

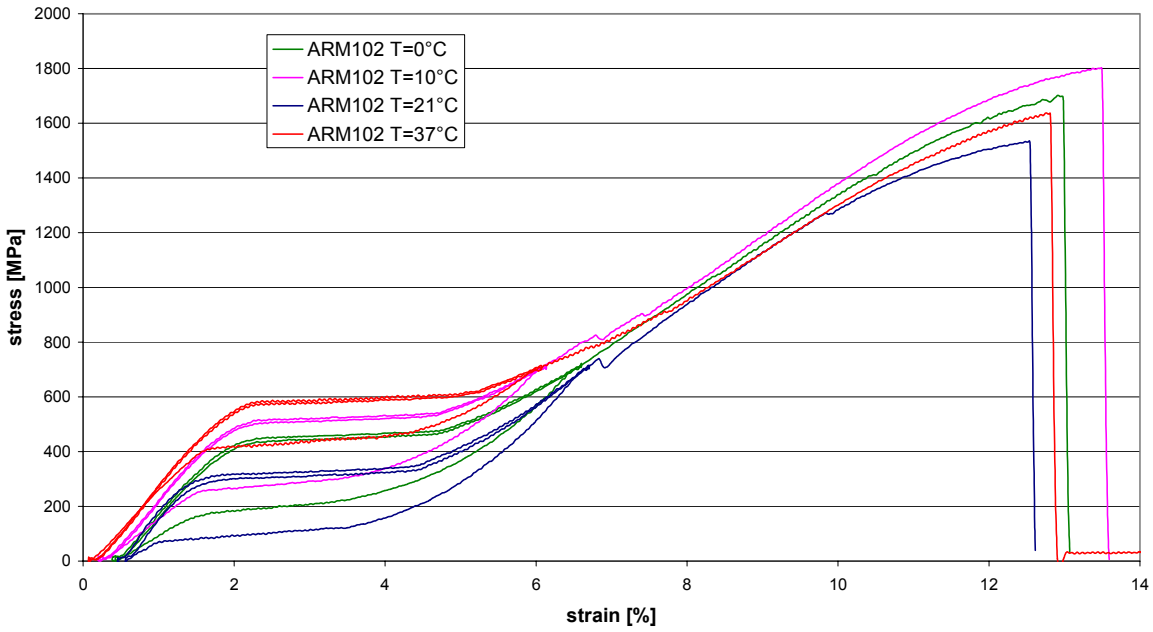

Fig.4.6: Temperature influence on Nitinol wire at the strain rate of $\dot{\varepsilon} = 0.017 \frac{1}{\text{sec}}$

The 200 cycles test was performed, at 37°C, to analyse the fatigue behaviour of Nitinol. In Fig 4.7, one ARM0102 wire specimen was cycled 200 times at the high strain rate of $\dot{\varepsilon} = 0.017 \frac{1}{\text{sec}}$. Between first and second cycle, the plateaux stresses decrease. After the second cycle the stress decrease became smaller than the decrease between the first and second cycle. The stress-strain loops (2^{nd} to 4^{th}) were nearly stabilized. The magnitude of plateaux stress values decreases with the number of cycles increase.

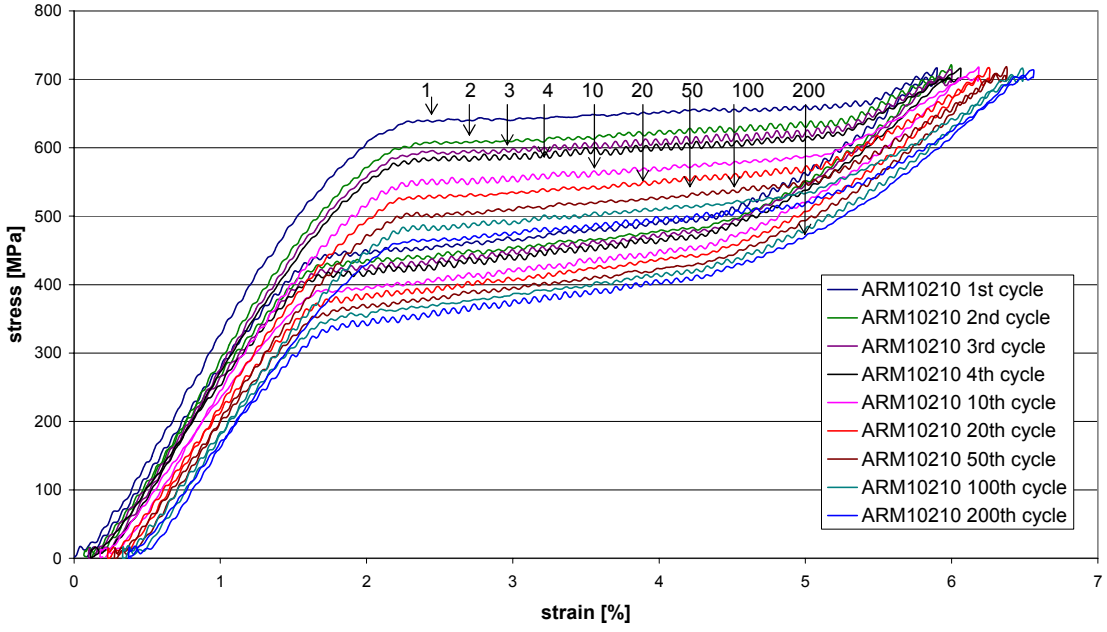

Fig.4.7: Number of cycle influence on Nitinol wire at the strain rate of $\dot{\varepsilon} = 0.017 \frac{1}{\text{sec}}$

4.1.2 FEM - SMA wire tensile test

FE analysis of tensile test of Nitinol wires was performed in order to verify the FE model and the constitutive material model. A tensile test FE model was developed in ADINA (see Fig 4.8). The material model for shape memory alloys from Meissner [9]was employed to describe shape memory and superelastic properties of Nitinol. Young's modulus values of the experimental data can be utilised as input data for the SMA material model. The Young's modulus data are the average value of 3 tests which have been carried out under same condition. The other required values are given from Medtronic or were assumed based on the parameter table from Meissner [9]. Tab 4.2 present the required import data for the ADINA program.

Tab.4.2: Table of identified parameter for the FEM SMA user-subroutine material model

Input values of material properties	Explanation of Input values		Nitinol parameterset from sebast Thesis [1]	Nitinol parameterset from experimental tensil test		Nitinol parameterset from MEDTRONIC	Nitinol final input parameterset	
				ARM0102	ARM0103		ARM0102	ARM0103
E_a [GPa]	CTI(1)	YOUNG*S MODULUS AUSTENITE	29.92	34121+/-1255	20201			
v_a []	CTI(2)	POISSON*S RATIO AUSTENITE	0.33			0.46	0.46	0.46
E_m [GPa]	CTI(3)	YOUNG*S MODULUS MARTENSITE	15.16	16947+/- 245	11296			
v_m []	CTI(4)	POISSON*S RATIO MARTENSITE	0.33			0.46	0.46	0.46
C_a [MPa/K]	CTI(5)	AUSTENITE TRANSFORMATION C	9				9	9
C_m [Mpa/K]	CTI(6)	MARTENSITE TRANS C	7.2				7.2	7.2
As [°C]	CTI(7)	AUSTENITE START OF TRANS T	25				3	3
Af [°C]	CTI(8)	AUSTENITE END OF TRANS T	52			35+-5	30	30
Ms [°C]	CTI(9)	MARTENSITE START OF TRANS T	−15				-37	-37
Mf [°C]	CTI(10)	MARTENSITE END OF TRANS T	− 33				-55	-55
Cr	CTI(11)	RE-ORIENTATION CONSTANT	0				0	0
Sr	CTI(12)	RE-ORIENTATION STRESS LIMIT	100				100	100
el	CTI(13)	MAXIMUM TRANSFORMATION STRAIN	0.0459				0.0459	0.0459

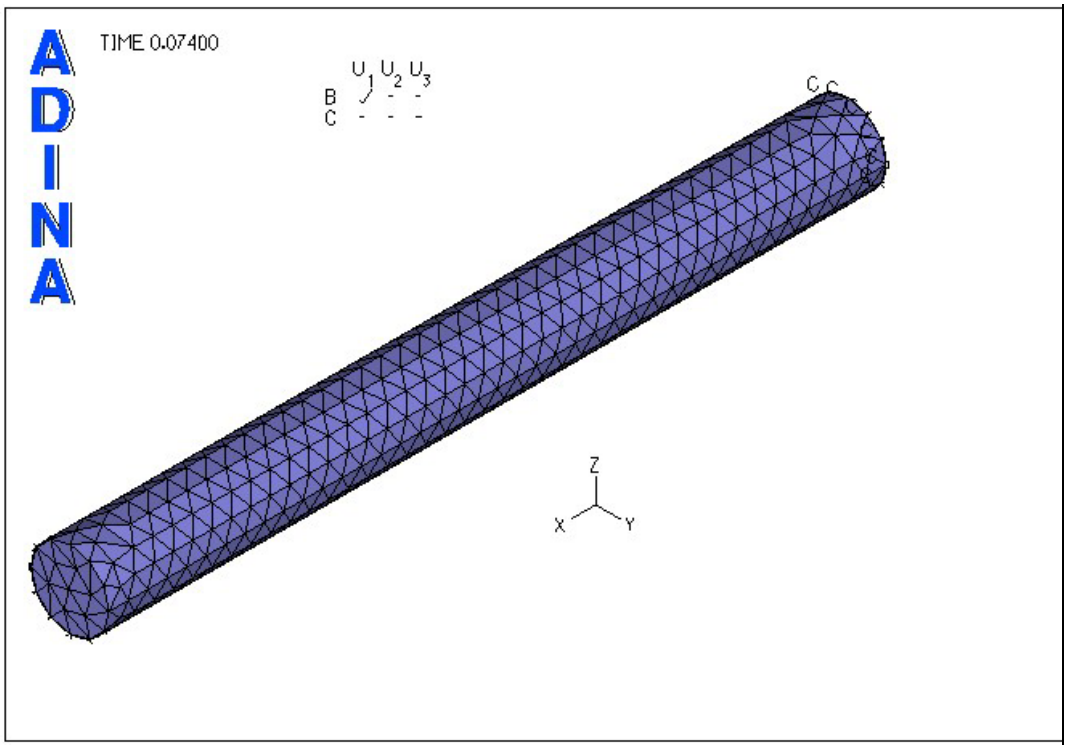

Fig.4.8: The tensile test FE model (shaded display) developed in ADINA

Figure 4.9 present the response graph of the numerical tensile test of an ARM0103 wire with defined Nitinol material properties. The curve verified the superelastic capability of the constitutive material model by showing reversible stress-induced austenite-martensite phase transformation.

Figure 4.10 presents the comparison of experimental and FEM wire tensile test (ARM0103). The stress-strain data of the FEM tensile test follows closely the experimental data. The best result is achieved with the FEM ARM0103 0.5mm 4-node. The influence of the length of the simulation wire is insignificant. However, the element type controls the result: The density of 4-nodes mesh is higher than the 8-nodes mesh because of the element shape, thus the results are more accurate.

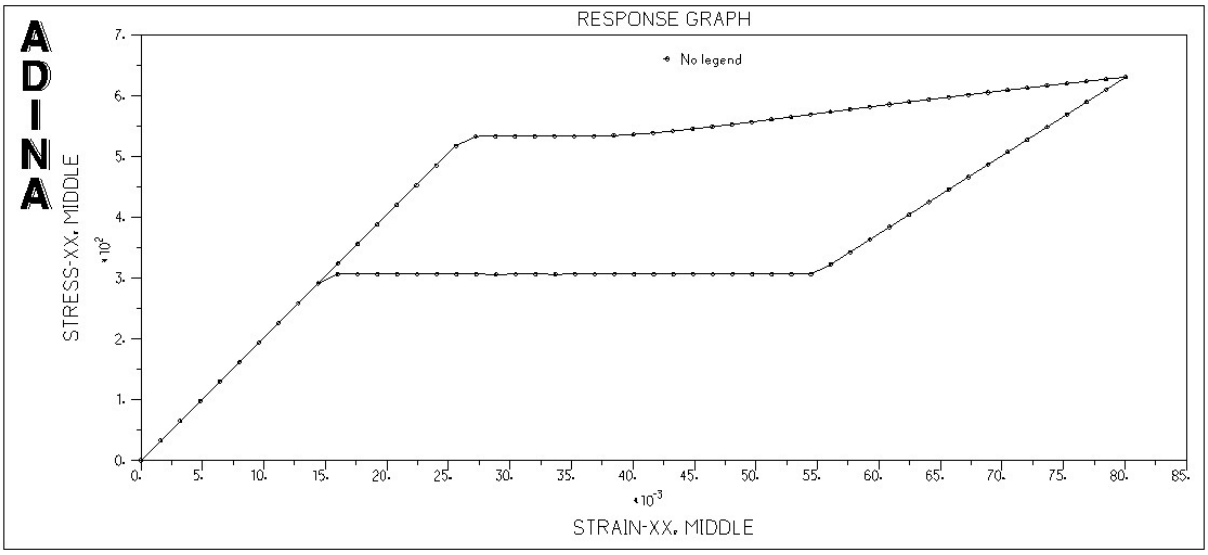

Fig.4.9: Strain-stress curve predicted by numerical simulation of Nitinol wire (ARM0103) with the mechanical properties data determined with the experimental tensile test.

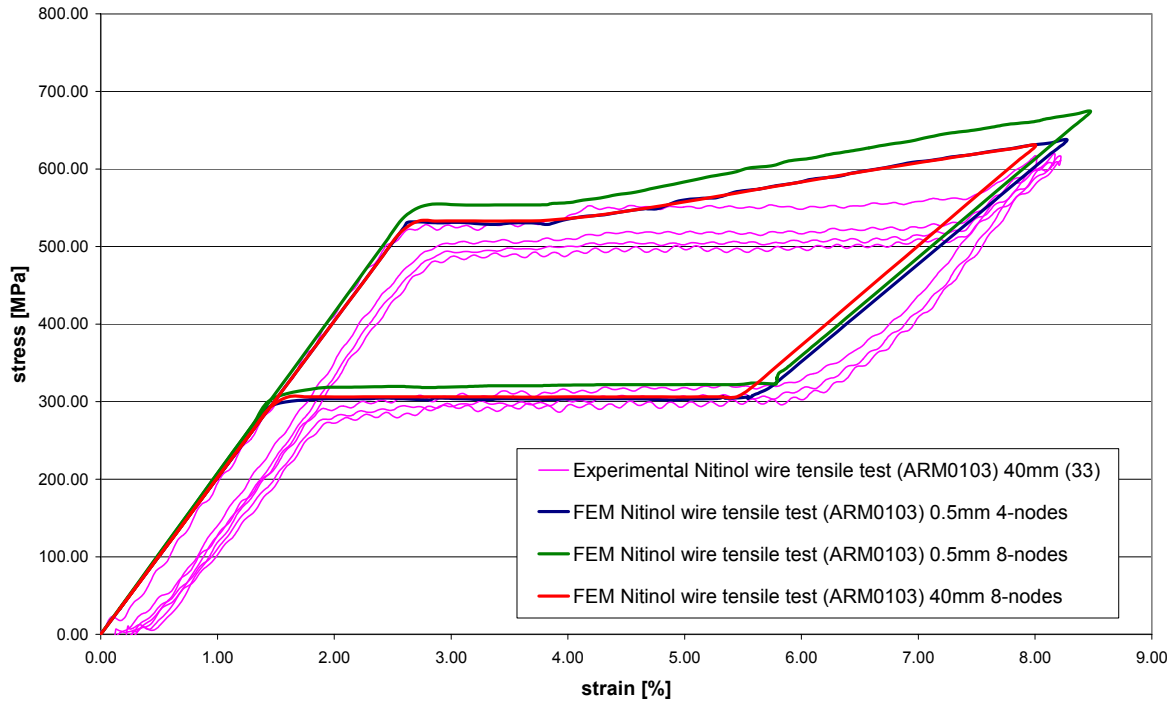

Fig.4.10 Comparison of experimental and FEM wire tensile test (ARM0103). The displayed wires vary in length and constitutive element types. The numerical stress-strain data correlates closely with experimental data.

The comparison stress-strain curves of the experimental tensile test and the FEM experimental tensile test of ARM0102 Nitinol wires is presented in Figure 4.11. The model solution follows the physical solutions reasonably. The best result is achieved with the FEM ARM0102 0.5mm 8-node which disagree the statement from the comparison of the experimental and FEM wire tensile test of the ARM0103 Nitinol wire. The influence of the length of the simulation wire is insignificant.

The simulations of the wire tensile test were carried out to prove the results accuracy. As the stress-strain data of the numerical model correlate with the experimental data, the constitutive material model and the material properties set of ARM0102 is used for the further FE Nitinol structure models.

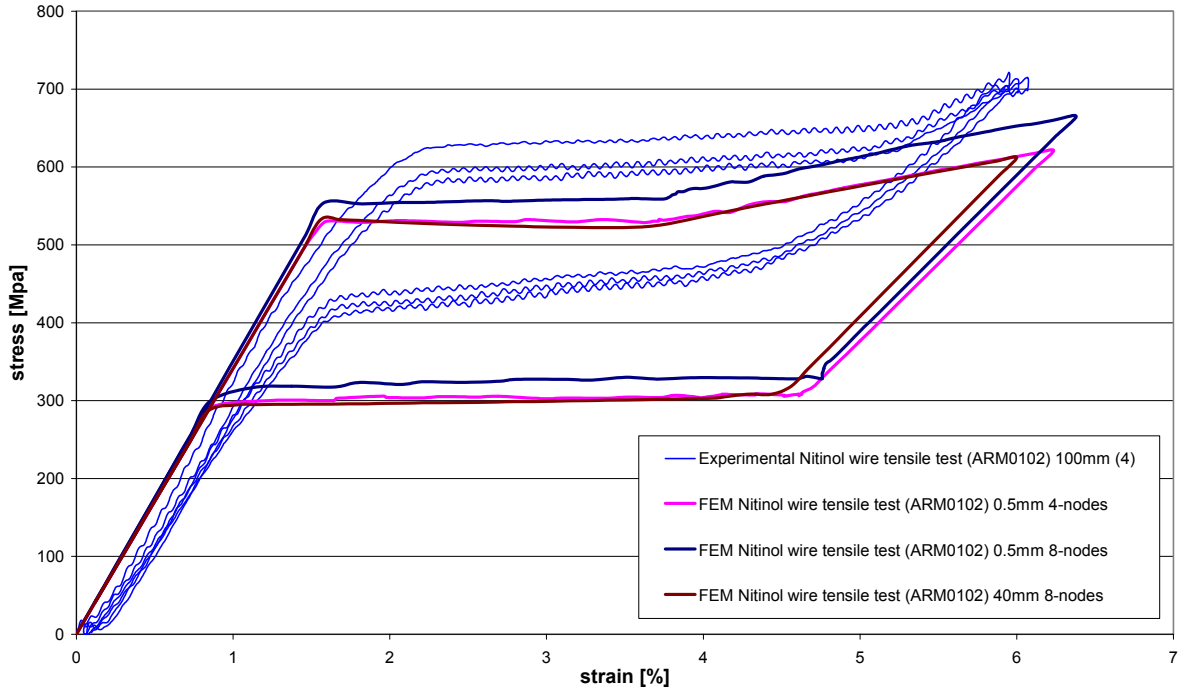

Fig.4.11 Comparison of experimental and FEM wire tensile test (ARM0102). Numerical results follow the physical solutions reasonably.

4.2 Helical Nitinol reinforcement model with Latex liner

Three-dimensional geometrical models of the Nitinol structures were created in Pro Engineer Wildfire, converted and then imported into ADINA. The FE model comprises a helical reinforcement Nitinol structure, a tubular Latex structure and a fluid model (see Figure 4.12). A normal traction was applied to the fluid mesh to approximate the blood pressure profile of a cardiac cycle. FEA was used to calculate the strain and stress field in the whole model and to interpret the stress and compliance results of the helical reinforcement structure in combination with the latex. By considering the entire numerical results of the helical reinforcement Nitinol FE model, the following results are indicated:

- The dilation of the structure in response to the internal fluid pressure was observed. Thus, the fluid interacted with the Latex structure.
- A mechanical deformation of the helical reinforcement structure was observed indicating properly working contact mechanism between Latex structure and the helical reinforcement structure.
- The results including stress values and displacement values of the whole FE model can be listed and/or graphed and are available for further analysis.

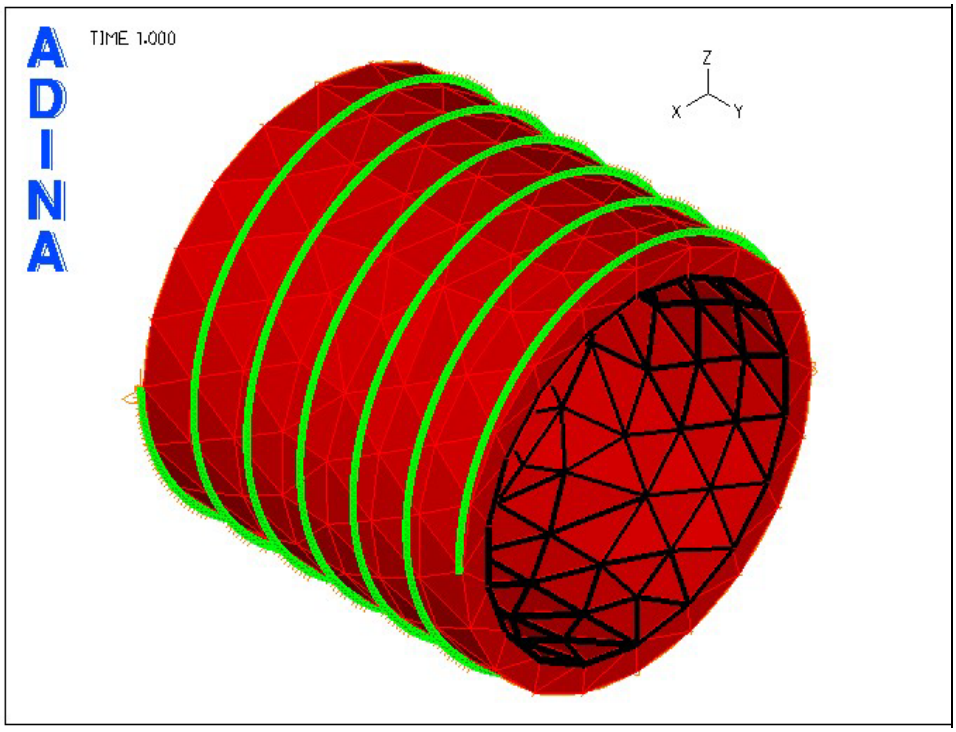

Fig.4.12 3-D FE model (shaded display) comprising a helical reinforcement Nitinol structure and a tubular Latex structure developed in ADINA. Black lines represent the Fluid structure boundaries.

Stress analysis

One aim of the stress analysis was to evaluate the stress values of the helical reinforcement structure caused by the fluid pressure. The success of cardiovascular prostheses depends on the capability of the structure to resist failure due to the applied load. The maximum stress value of the helical reinforcement structure must not exceed the ultimate tensile stress of the material, i.e. Nitinol.
A stress band plot of the FE model comprising a helical reinforcement structure and tubular Latex structure were created in ADINA. Figure 4.13 shows the graphical representation of the stress values of each element within the structure. As the stresses of the helical Nitinol reinforcement structure are of interests, solely a band plot of the structure without the Latex was analysed by defining a zone which contains the elements of the Nitinol structure only

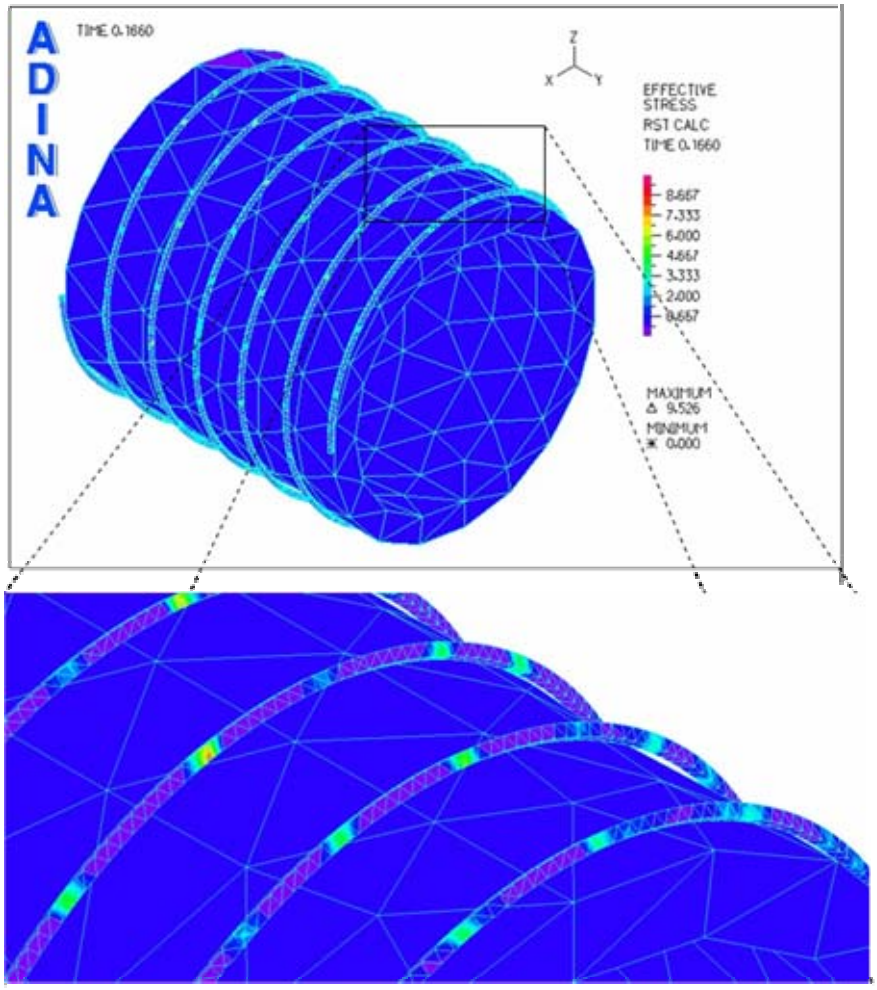

Fig.4.13: Band plot of the FE model comprising a helical reinforcement structure and tubular Latex structure developed in ADINA. The figure shows the graphical representation of the stress values of each element within the structure.

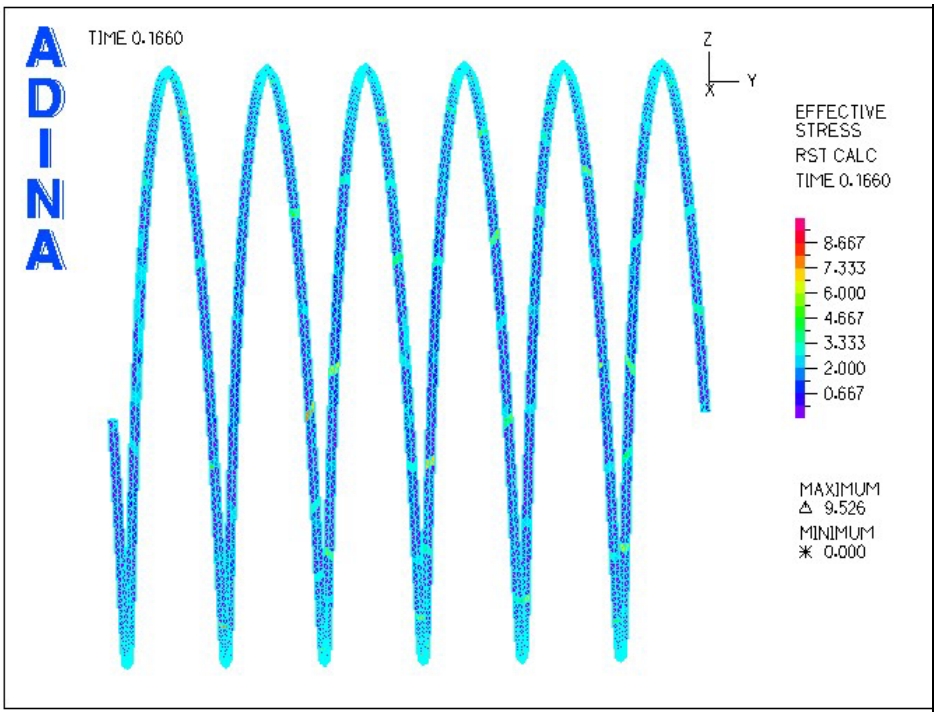

Fig.4.14: Stress band plot of helical Nitinol reinforcement structure. The maximum stress value $\sigma_{\max} = 9.53 \frac{N}{mm^2}$ of the structure were observed at the maximum pressure of p=119.28mmHg.

The minimum and maximum values of the stress band plot are displayed in Figure 4.14. The maximum stress value of the helical reinforcement structure was detected as:

$$\sigma_{\max} = 9.53 \frac{N}{mm^2} = 9.53 MPa$$

The average ultimate tensile stress value was determined from the experimental tensile test of the Nitinol wire to be as follows:

$UTS = 1681.55 \pm 33.44 MPa$ (ARM0102 samples)

Comparing the maximum stress value of the helical reinforcement structure predicted by FEA to the experimental average ultimate tensile stress values shows that the stresses in the helical structure were smaller than the ultimate tensile stress values of the Nitinol wire. Therefore, the failure of the helical Nitinol reinforcement structure caused by the fluid pressure, approximating the blood pressure profile of a cardiac cycle, can be excluded.

Compliance analysis

The radial dilation of the structure is another important aspect in the analysis of the mechanical behaviour of the cardiovascular prostheses. The displacement in radial direction of the helical Nitinol reinforcement was determined. From the results of the displacement values of the Latex structure, the compliance of the Latex liner surrounded by the helical Nitinol reinforcement was calculated. The compliance data of the reinforced Latex liner was subsequently compared to the numerically predicted compliance of a Latex liner without the helical reinforcement and to compliance data from the literature (see chapter 4.4).

The FE model represents solely the half of the entire structure by utilising symmetry conditions. The “free"end of the model represents the mid-section of the entire model. It was assumed that at the mid-section the influence of numerical, and physical, boundary conditions can be neglected. The results of the displacement in radial direction at the mid-section of the helical reinforcement and of the Latex structure FE models were analysed and are listed in Table.4.3. The radial displacement magnitudes are presented at three pressure stages, p = 0; 80.7; 119.3mmHg. The displacement magnitudes of the Latex liner and of the helical reinforcement increased with increasing pressure.

Tab.4.3: Comparison of the radial displacement magnitudes of the mid-section of the Latex liner and helical reinforcement depending on the pressure

Pressure [mmHg]	Pressure [Pa]	Time [sec]	Radial displacement magnitude of Latex liner [mm]	Radial displacement magnitude of helical reinforcement [mm]
0	0	0	0	0
80.72	10761.54	0.66	2.95×10^{-5}	1.85×10^{-5}
119.28	15902.46	0.17	4.36×10^{-5}	2.73×10^{-5}

The displacement-time curve (Figure 4.15) of the Latex liner and of the helical reinforcement structure showed that the displacement changed cyclically following the applied pressure/normal traction curve as it is presented in Figure 3.8. The Latex material and the helical Nitinol structure deformed according to pressure profile which approximates the blood pressure profile of a cardiac cycle due to the applied Fluid-Structure-Interaction boundary condition and master/slaves constrains. Due to the different Young’s moduli of the Latex structure and the helical reinforcement structure, respectively, and the different structure design, the displacement magnitude of the Latex liner was higher than those of the helical reinforcement structure. It is assumable that the Latex liner expanded in the spaces between the helical reinforcement. The contact mechanism and the master/slaves constrains forced the helical reinforcement to deform accordingly to the Latex liner.

The displacement results served as basic for the compliance calculation for the braided stent and for the latex liner which has been carried out (see Table 4.4).

Table 4.4: Overview of calculated diameter values for Latex liner and helical reinforcement

Pressure [mmHg]	Time [sec]	Radial displacement magnitude of Latex liner [mm]	Diameter values of Latex liner [mm]	Radial displacement magnitude of helical reinforcement [mm]	Diameter values of helical reinforcement [mm]
0	0	0	2.9492	0	3.0492
80.72	0.66	2.95E-5	2.949259	1.85E-05	3.049237
119.28	0.17	4.36E-05	2.949346	2.73E-05	3.049292

Compliance of helical Nitinol reinforcement was analyzed as:

$$C_d = \frac{d_{sys} - d_{dia}}{d_{dia}} \times \frac{100}{P_{sys} - P_{dia}} \times 100 = 0.0045 \frac{\%}{100 mmHg} \tag{4.1}$$

Compliance of the Latex liner with helical reinforcement was determined as:

$$C_d = \frac{d_{sys} - d_{dia}}{d_{dia}} \times \frac{100}{P_{sys} - P_{dia}} \times 100 = 0.0074 \frac{\%}{100 mmHg} \tag{4.2}$$

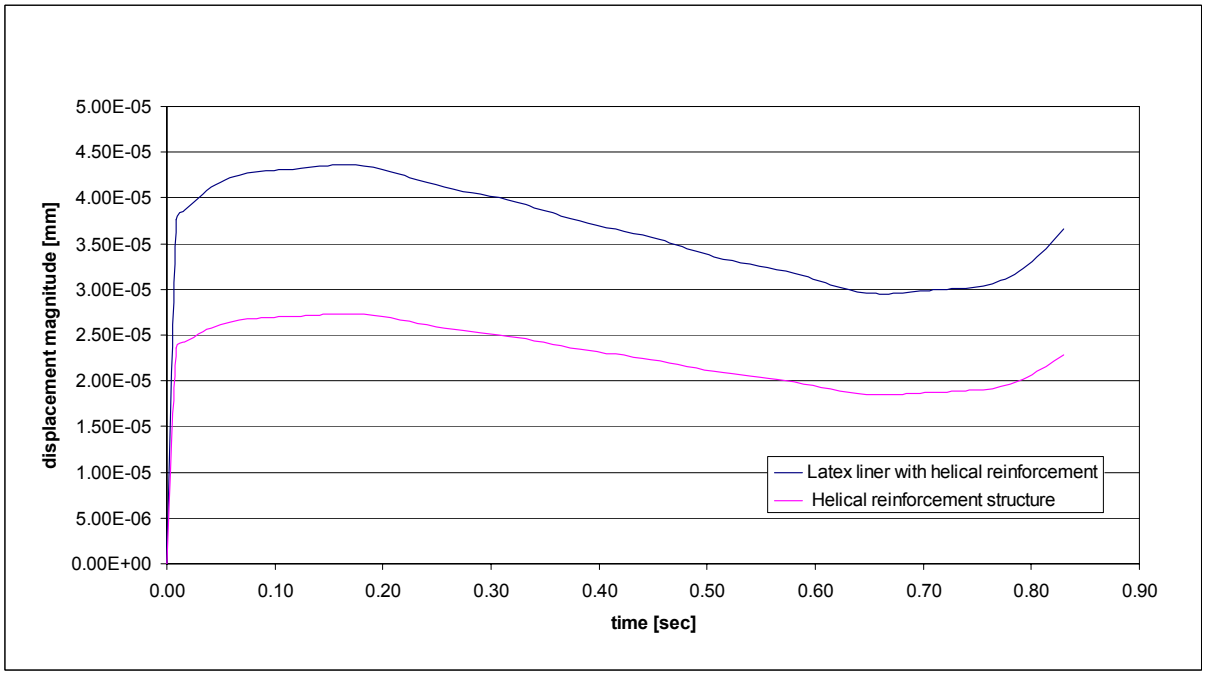

Fig.4.15: Displacement magnitudes on the free end of Latex Liner compared to those of the helical reinforcement structure depending on the time. Contact mechanism and the Master/Slaves constrains forced the structure to deform accordingly to the Latex liner.

4.3 Braided stent model with Latex Liner

A three-dimensional geometrical model of a braided Nitinol structure was created in Pro Engineer Wildfire, converted and then imported into ADINA. The FE model comprises a braided Nitinol stent structure, a tubular Latex structure and a fluid model (see Figure 4.16). The loading condition of the model was defined in the same way as in the helical Nitinol reinforcement model. A normal traction was applied to the fluid mesh to approximate the blood pressure profile of a cardiac cycle. A Finite analysis has been carried out to evaluate the stress and compliance of the braided stent structure in combination with the latex liner. By considering the entire numerical results of the braided stent Nitinol FE model, the following observations can be stated:

- The dilation of the Latex structure in response to the internal fluid pressure was observed. Thus, the Fluid interacted with the Latex structure.
- A mechanical deformation of the braided Nitinol structure was observed indicating properly working contact mechanism between Latex structure and braided Nitinol structure.
- The results including stress values and displacement values of the whole FE model can be listed and/or graphed and are available for further analysis.

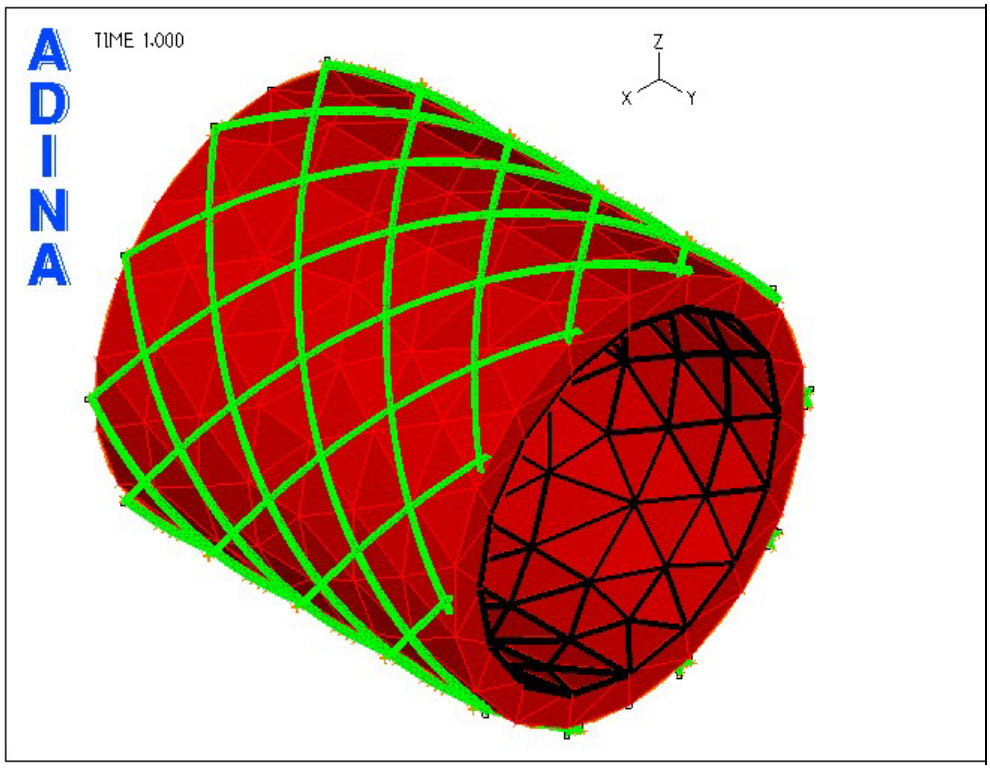

Fig.4.16: 3-D FE model (shaded display) comprising a Nitinol stent structure and tubular Latex structure developed in ADINA. The fluid-structure Boundaries are presented by black lines.

Stress analysis

Furthermore, in the braided stent model, a stress analysis was performed with the aim of evaluating the stress acting in the braided stent structure caused by the fluid pressure. The maximum stress value of the braided stent structure must not exceed the ultimate tensile stress of the material, the Nitinol, to prevent failure.

Figure 4.17 shows the graphical representation of the stress of each element of the model. A band plot with magnification of the displacement of the structure without the Latex liner is shown in Figure 4.18. The figure indicates the stent structure expanded uniform in radial direction. Furthermore, the influence of the fixed boundary condition of the Latex liner, limited the uniform expansion of the stent in longitudinal direction due to the applied master/slaves constrains.

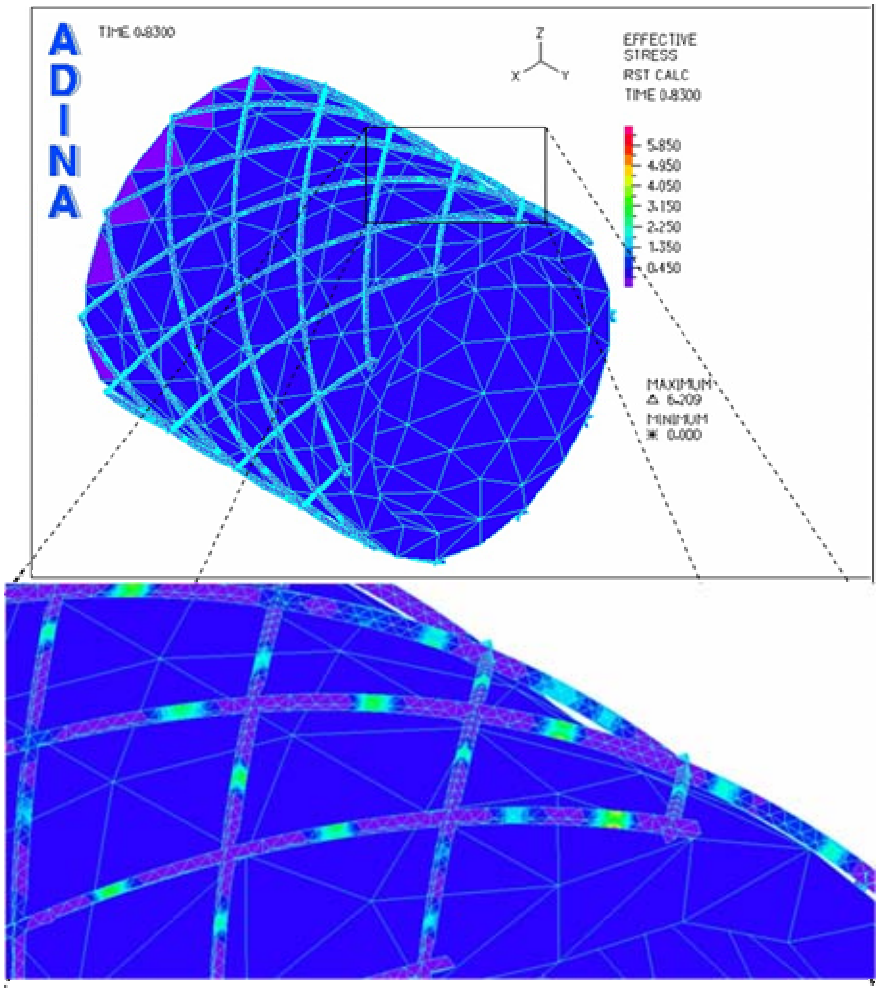

Fig.4.17: Band plot of the FE model comprising a Nitinol stent structure and tubular Latex structure developed in ADINA. The figure shows the graphical presentation of the stress values of each element within the structure.

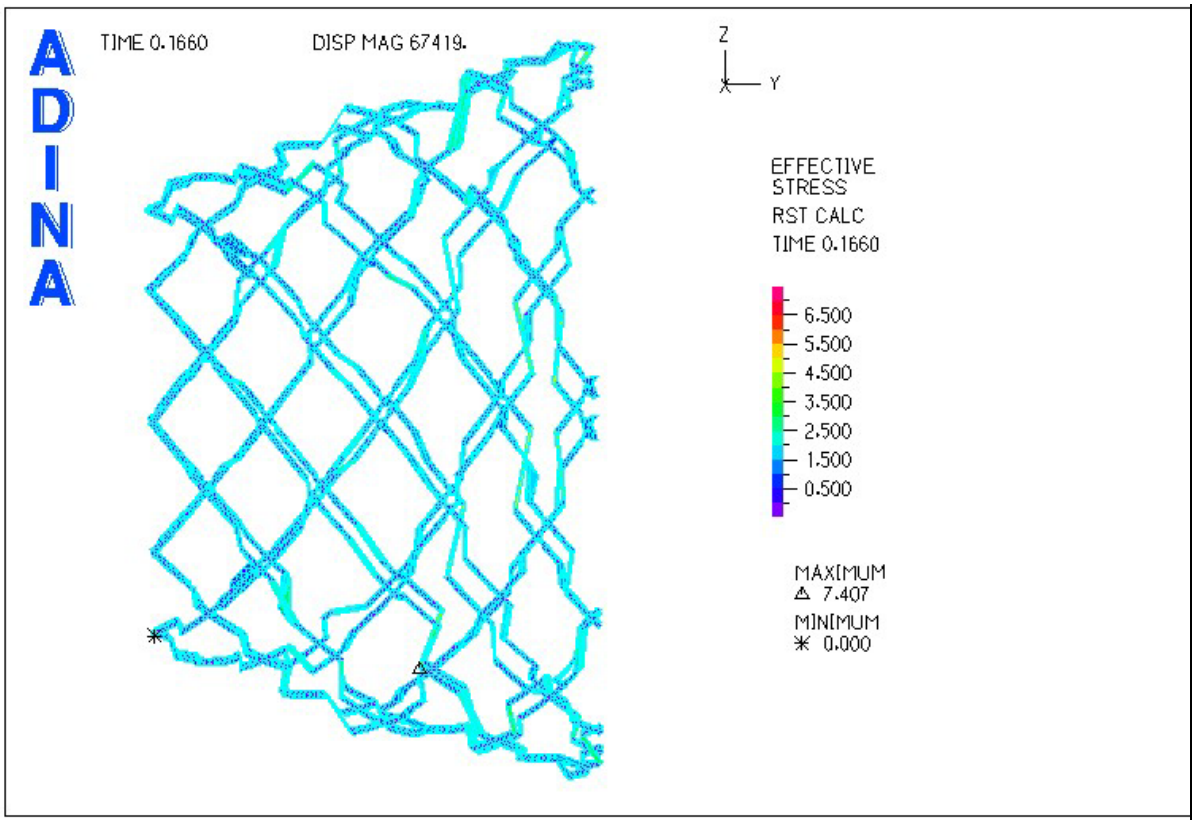

Fig.4.18: Stress band plot of Nitinol stent structure with magnified deformation. The maximum stress values of the structure were detected at the pressure of p=119.28mmHg from the band plot. Uniform expansions of the stent in longitudinal direction were limited by the fixed boundary condition of the Latex liner.

Figure 4.18 displays the minimum and maximum values of the stress in the stent structure. The maximum stress value was predicted to be:

$$\sigma_{\max} = 7.41 \frac{N}{mm^2} = 7.41 MPa$$

An average ultimate tensile stress $UTS = 1681{,}55 MPa$ was determined from the experimental Nitinol wire tensile test. Thus, the maximum stress in the stent structure was smaller than the ultimate tensile stress of the Nitinol wire. Failure of the stent structure caused by the fluid pressure, approximating the blood pressure profile of a cardiac cycle, can be excluded.

Compliance analysis

A compliance analysis, similar to that of the helical Nitinol reinforcement model, was performed. From the displacement predicted for the Latex structure reinforced by the braided stent structure, the compliances of braided stent structure and of the Latex liner were calculated. A compliance comparison and a verification of the compliance data are presented in chapter 4.4.

The results of the displacement in radial direction at the mid-section of the braided stent structure and of the Latex structure FE models were analysed and are listed in Table.4.5. The radial displacement magnitudes are presented at three pressure stages, p = 0; 80.7; 119.3mmHg. The displacement magnitudes of the Latex liner and of the braided stent structure increased with increasing pressure

Tab.4.5: Comparison of the radial displacement magnitudes of the mid-section of the Latex liner and the braided stent structure on the pressure

Pressure [mmHg]	Pressure [Pa]	Time [sec]	Radial displacement magnitude of Latex liner [mm]	Radial displacement magnitude of braided stent [mm]
0	0	0	0	0
80.72	10761.54	0.66	8.89×10^{-6}	8.35×10^{-6}
119.28	15902.46	0.17	1.31×10^{-5}	1.24×10^{-5}

The displacement-time curve (Figure 4.19) of the Latex liner and of the braided stent structure showed that the displacement changed cyclically following the applied pressure/normal traction curve as it is presented in Figure 3.11. Due to the different Young's moduli of the Latex structure and the braided stent structure, respectively, and the different structure design, the displacement magnitude of the Latex liner was higher than those of the braided stent structure. Figure 4.20 presents the displacement magnitudes of the Nitinol braided stent at the pressure of p=119.28mmHg. It is assumable that the Latex liner expanded in the spaces between the braided stent. The contact mechanism and the master/slaves constrains forced the braided stent to deform accordingly to the Latex liner.

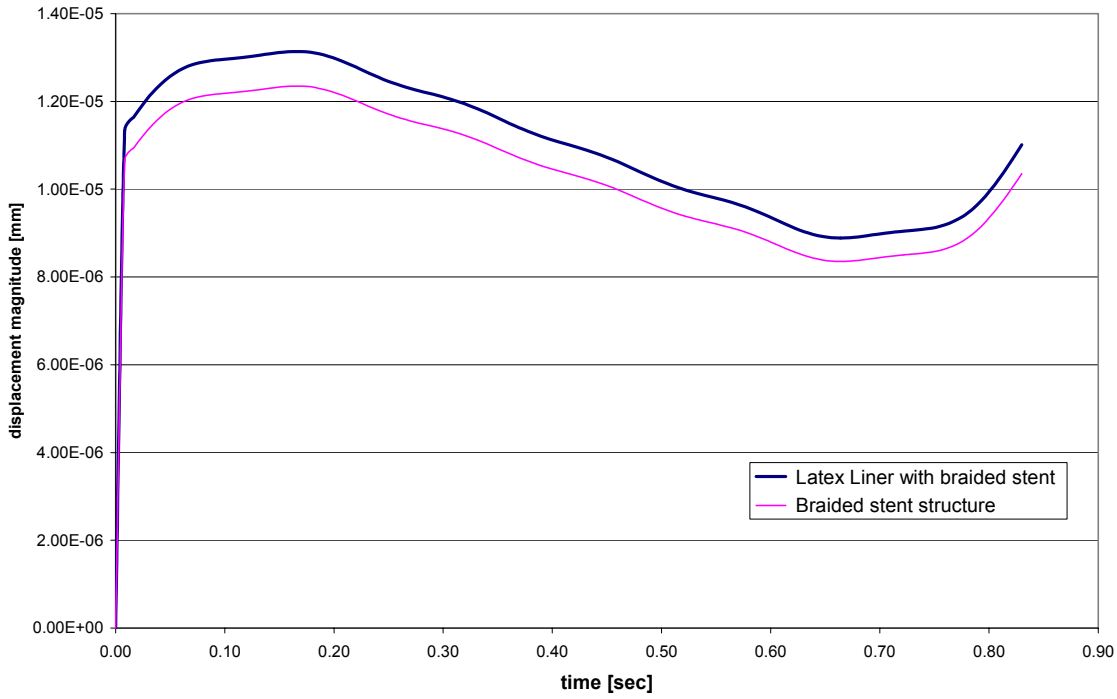

Fig.4.19: Displacement magnitudes versus time at themed-section end Latex Liner and the Nitinol braided stent structure.

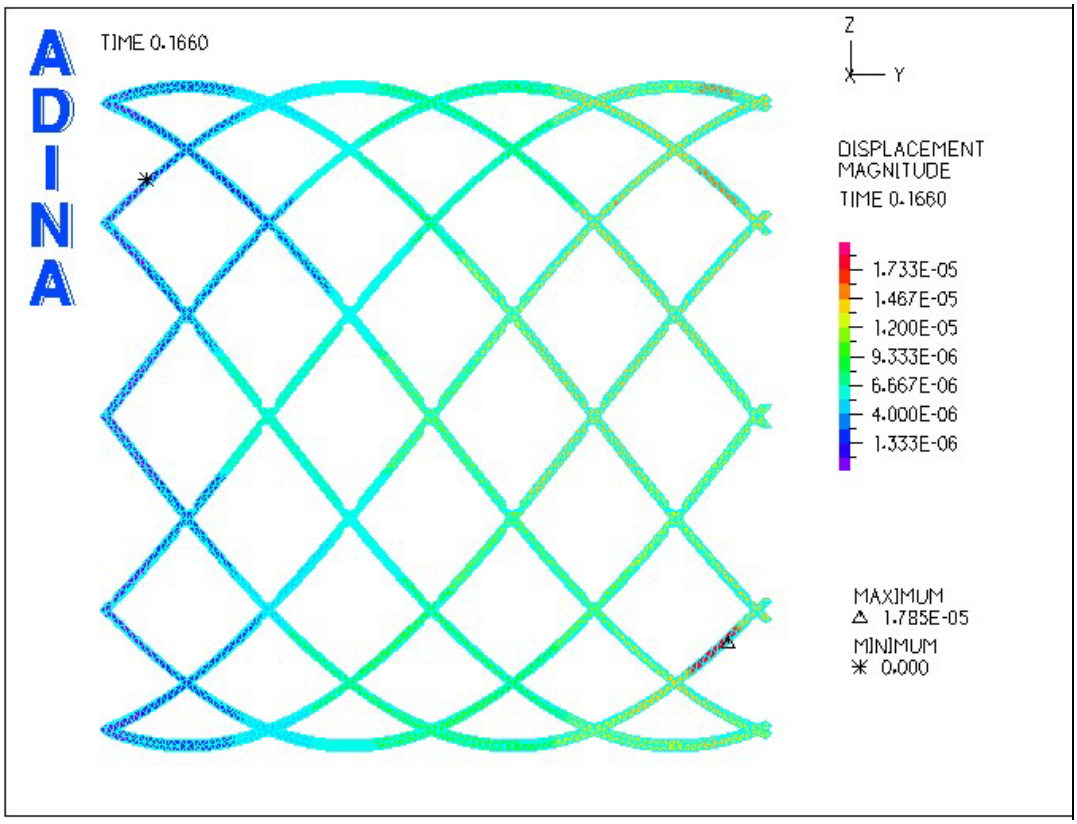

Fig.4.20: Displacement magnitudes of the Nitinol braided stent at the pressure of p=119.28mmHg.

Additionally, two nodes positioned approximated at a length of l=1.5 mm from the mid-section, where the influence of the fixed boundary condition is existent, were chosen to analyse the deformation of the latex structure. One node of the Latex liner, node A, situated underneath a Nitinol wire and one node of the Latex liner, node B, situated in a region between Nitinol wires were analysed (see Figure 4.21). The stress and strain values were determined at the pressure of p = 80.7 mmHg and p = 119.3mmHg.

The following stress values were determined:

- p = 80.7 mmHg

  Node A: $\sigma = 5.78 \times 10^{-5}\, MPa$

  Node B: $\sigma = 1.24 \times 10^{-4}\, MPa$

- p = 119.3 mmHg

  Node A: $\sigma = 8.54 \times 10^{-5}\, MPa$

  Node B: $\sigma = 1.84 \times 10^{-4}\, MPa$

The following strain values were determined:

- p = 80.7 mmHg

  Node A: $\varepsilon = 1.13 \times 10^{-4}\%$

  Node B: $\varepsilon = 3.01 \times 10^{-4}\%$

- p = 119.3 mmHg

  Node A: $\varepsilon = 1.67 \times 10^{-4}\%$

  Node B: $\varepsilon = 4.45 \times 10^{-4}\%$

Higher stress and strain values were predicted for the Latex region between Nitinol wires compared to the Latex region underneath a Nitinol wire for either pressure value. This indicates that the Latex liner expanded more in the spaces between the Nitinol wires of the braided stent than in a region underneath a Nitinol wire.

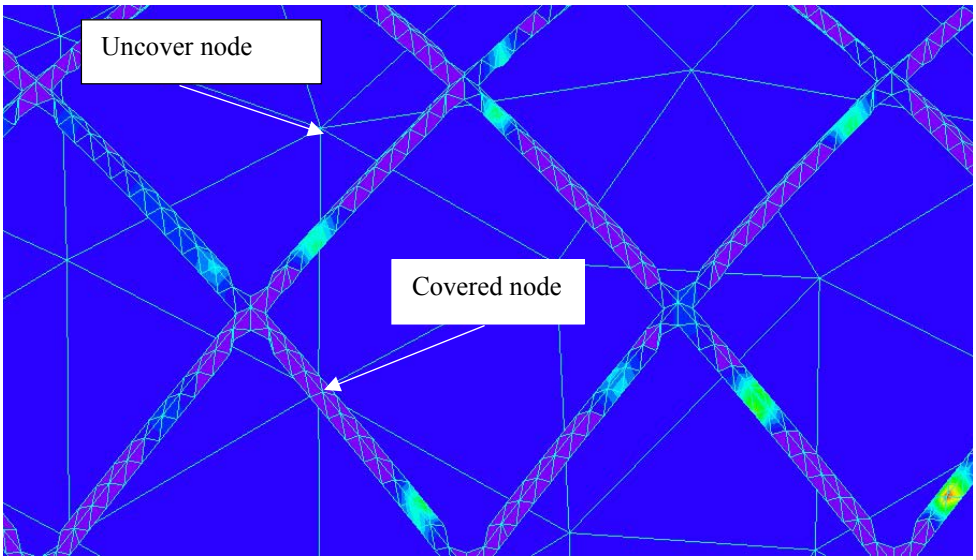

Fig.4.21: Illustration of the two nodes to analyse the deformation of the latex structure in contact with the stent structure.

The displacement results served as basic for the compliance calculation for the braided stent and for the latex liner which has been carried out (see Table 4.7).

Table 4.7: Overview of calculated diameter values for Latex liner and braided stent

Pressure [mmHg]	Time [sec]	Radial displacement magnitude of Latex liner [mm]	Diameter values of Latex liner [mm]	Radial displacement magnitude of braided stent [mm]	Diameter values of braided stent [mm]
0	0	0	2.9492	0	3.0492
80.72	0.66	8.89E-6	2.94921778	8.35E-06	3.049217
119.28	0.17	1.31E-05	2.949244	1.24E-05	3.049242

Compliance of braided stent structure was analyzed as:

$$C_d = \frac{d_{sys} - d_{dia}}{d_{dia}} \times \frac{100}{P_{sys} - P_{dia}} \times 100 = 0.0020 \frac{\%}{100 mmHg} \tag{4.3}$$

Compliance of the Latex liner with braided stent was determined as:

$$C_d = \frac{d_{sys} - d_{dia}}{d_{dia}} \times \frac{100}{P_{sys} - P_{dia}} \times 100 = 0.0022 \frac{\%}{100 mmHg} \tag{4.4}$$

4.4 Compliance comparison and verification

The maximum stress values in the two Nitinol structures were much smaller than the ultimate tensile stress (UTS) of the comprising Nitinol material. Therefore, the failure of Nitinol can be excluded. For further evaluation of Nitinol structures and verification of numerical results, the determined compliance values are used. Table 4.8 gives an overview of determined compliances values.

Table.4.8: Comparison of compliance of Latex liners and Nitinol structures.

Condition	Compliance [%/100mmHg]
Helical reinforcement structure	0.0045
Braided stent structure	0.002
Latex liner without reinforcement structur	4.84
Latex liner with the helical reinforcement structure	0.0074
Latex liner with the braided stent structure	0.0022
Latex liner without reinforment experimental result [5]	17.7

Braided stent structure vs. helical reinforcement structure

The compliance of the braided stent structure was compared to the compliance of the helical reinforcement structure. The compliance of the helical reinforcement structure was 2.25 times bigger than the compliance of the braided stent structure. Therefore, the braided stent structure design was stiffer than the helical reinforcement structure. As the intersections of the Nitinol wires within the braided stent structure were merged in the Pro/Engineer geometry model, the structure became a stiff structure and the difference in the compliance data seems to be reasonable. The helical reinforcement structure allowed the Latex liner to expand more than the braided stent structure. Thus, the structure design was more flexible to the Latex liner expansion. Other factors which influence the compliance are the number of pitches of the helical reinforcement and the number of wires which are incorporated into the braided stent structure. Further work has to be focused on the influence factors.

Latex without reinforcement: numerical vs. experimental

Compliance of a Latex liner without reinforcement tested in experimental compliance tests in [5] were compared with the numerical determined compliance of a Latex liner without reinforcement of this work. The experimental determined compliance of a Latex liner was 3.66 times higher then the compliance of a Latex liner determined through numerical simulation. A reason for this difference is the limitation of the Latex FE model length (l=3mm). It is assumable that the fixed boundary conditions had an influence on the expanding behaviour of

the Latex liner, so that the detected displacement magnitude on the mid-section Latex side, used for the compliance calculation, has not reached the maximum magnitude.

Nitinol structure vs. Latex liner with reinforcement

The compliance of the Nitinol structures were compared to the compliance of the Latex liners which were reinforced by the Nitinol structure. The compliance of the Latex liners were bigger than the compliance of the Nitinol structures. Therefore, the Latex liners expand more than the Nitinol structures. Through the comparison of two nodes of the Latex, node A situated underneath a Nitinol wire of the braided stent and node B situated in a region between Nitinol wires, it was stated that the Latex liner expanded more in the spaces between the Nitinol wires of the braided stent than in a region underneath a Nitinol wire. The compliance of the Nitinol structures and of the Latex liners were calculated with the maximum displacement values, respectively, what explains the higher compliance of the Latex liner.

5 Discussion

Fluid-Structure-Interaction in the simulation of cardiovascular prostheses:

3D FSI models with multicomponents (Latex, prostheses structure) are difficult to solve. The interaction of the fluid and the structure is very complex, and sensitive to many controlling parameters in the FE analysis software. The FE models were simulating an experimental set-up for compliance measurements where water is used as the fluid. Therefore, Transient steady flow was simulated without considering turbulence, compressibility and viscosity changes which are involved in blood flow simulation.

Stress/compliance analysis

The stress/compliance analysis of the FEM models should give an idea of the mechanical behaviour of cardiovascular prostheses. The results are depending on the used Nitinol material properties of the prostheses structure. The 13 SMA materials properties which are required for the material model in ADINA, are a mix of experiment values, values from the literature and assumption. Thus, the numerical prediction of the compliance of the Nitinol structures doesn't correspond to reality.

Reliability and Accuracy of Computational Results:

Many factors affect computational results and predictions: Geometry, material properties, loading and boundary conditions. However, also solver settings specifying analysis control parameters have an influence on the accuracy of the computational results. Proper model assumptions properties are essential for a reliable computational simulation. It is important to perform a bench mark for computational models to have confidence that the computational results are applicable, reliable, and accurate.

Model Limitations:

The computational models are depending on computational memory capacity. Due to these technical parameters, the choice of geometry dimensions (for example length of prostheses), element types, and mesh size is affected. These limitations need to be acknowledged so that the possibility of the computational predictions can be understood.

6 Conclusions and future prospects

This study describes the development of a Finite Element analysis tool to simulate and predict the mechanical behaviour of helical and braided tubular structures comprising Nitinol wires for the use in cardiovascular prostheses. Experimental tests were performed to determine the mechanical properties of Nitinol. FE analysis of tensile tests of Nitinol wires was performed to verify the FE models and the constitutive material model. The FE analysis of Nitinol structures was focused on stress and compliance analysis to determine the mechanical behaviour depending on different Nitinol design structures.

Experimental wire tensile tests

The mechanical properties, in particular, Young's modulus, stress-induced transformation stresses and strains, ultimate tensile stress and strain to failure, were determined from the analysis of the experimental tensile test data. The data verified the superelastic behaviour of the Nitinol wires at physiological body temperature showing a reversible stress-induced austenite-martensite phase transformation. The determined mechanical properties serve as input for the material model of the numerical tensile test.

Concerning the experimental set-up the following conclusions were indicated. Most of the wires broke in the middle zone after achieving the strain limit. The attaching method was satisfactory as the wires were tested without inducing prior stresses at the clamps.

FE tensile tests

To verify the constitutive material model, a FE analysis of tensile tests of Nitinol wires was performed. The numerical results showed stress-strain data which correlated closely with the experimental stress-strain data. Therefore, it was justified to apply the constitutive material model for the FE analysis of the helical and braided tubular structures.

FE analysis of helical reinforcement model and braided stent model

Three-dimensional geometrical models of Nitinol structures were created in Pro/Engineer wildfire. After converting and importing them into ADINA Finite Element software, they undergo a FE analysis. Stress and compliance analysis were performed for a better understanding of mechanical behaviour of helical and braided tubular structures comprising thin Nitinol wires for the use in cardiovascular prostheses. The FE models have the potential to use them for future design optimisation of cardiovascular prostheses prior to costly prototype studies in the development stage.

The stress analysis of the numerical results indicated stress values smaller than the ultimate tensile stress in the Nitinol structures. Therefore, the failure of the prostheses structure caused by the fluid pressure, approximating the blood pressure profile of a cardiac cycle, was excluded.

The numerical compliance analysis of the helical/braided Nitinol structures indicated the dilation of the structure in response to the fluid pressure. The Latex liner and the prostheses structures showed displacement curve shapes following the shape of the applied normal traction. With increasing pressure, the expansion of the Latex liner surrounded by the prosthesis structure, increased. The fluid interacted with the Latex structure and the prostheses structures and deformed accordingly to the latex structure due to the contact mechanism and master/slave boundary condition.

The compliance of a plain Latex liner was higher than the compliance of the helical reinforcement and braided stent structure, respectivly. The compliance of the helical reinforcement was due to its design being more flexible than the braided stent structure and therefore, showed a higher compliance. The comparison of numerical predicted compliance data from the literature indicated that the literature compliance data of a plain Latex liner was much higher than the plain Latex liner in this work. This indicated that improvements and further work has to be done.

Future prospects in the FE analysis of cardiovascular prostheses

Future work concerning FE tensile tests will be focused on performing more experimental tests to obtain proper material properties set. In particular the following tests should be performed:

- DSC (Differential Scanning Calorimeter) to measure the phase transformation temperatures of Nitinol wires by detecting the changes in heat flow in the alloy during phase transformation
- Experimental tensile test with special equipment for testing Nitinol wires. A temperature chamber, special wire clamps and precise detectors for the range of loads should be used to get more accurate results.

Future works concerning the simulation of cardiovascular prostheses will be focused on following emphases:

- Increasing the prostheses length to decrease the influence of the fixed boundary condition or defining boundary condition to stabilise the structures.
- Determination of material properties of SMA FE material model to obtain a consistent material set
- Optimisation of the braided stent Pro/Engineer geometry model so that the wires can move relatively to each other at the intersection
- Variation of fluid properties regarding the simulation of blood
- Variation of element types and mesh densities to obtain closer results
- Replacing the braided stent/ helical reinforcement structure with different stent designs to simulate and predict the mechanical behaviour of the prostheses
- Comparisons of the computational results with relevant experiments test data or literature

References

1. *Arteriosklerose*, medicine worldwide.
2. Rutten, M.C.M., *Fluid-solid interaction in large arteries*. 1998, Technische Universiteit Eindhoven.
3. Holzapfel, G.A.G., T.C.; Ogden, R.W., *A new constitutive framework for arterial wall mechanics and a comparative study of material models.* Journal of Elasticity, 2000. **61**: p. 1-48.
4. Fung, Y.C., *Biomechanics: mechanical properties of living tissues*. 2nd ed. 1993, New York: Springer.
5. Yeoman, M., *The design and optimisation of fabric reinforced porous prosthetic grafts using finite element methods and genetic algorithms*, in *Department of Mechanical Engineering*. 2004, University of Cape Town: Cape Town. p. 190.
6. Walker, R.S., R.; Sherriff,S.; Wood,R., *Latex vessels with customized compliance for use in arterial flow models.* Physiol. Meas., 1999. **20**: p. 277-286.
7. Bergel, D.H.S., d.L., *Arterial elasticity and fluid dynamics.* Progr. Biophys., 1971. **22**(1).
8. Belz, G., *Elastic properties and windkessel function of the human aorta.* Cardiovascular Drugs and Therapy, 1995. **9**: p. 73-83.
9. Meissner, S., *On Constitutive Modeling of Shape Memory Alloys within the Finite Element Method*, in *Mechanical Engineering*. 2004, Technical University of Munich: Munich. p. 83.
10. Kujala, S., *Biocompatibilty and biomechanucal aspects of Nitinol shape memory metal implants*, in *Department of surgery*. 2003, University of Oulu: Oulu. p. 90.
11. Lipscomb, I.P.N., L.D.M., *The application of shape Memory Alloys in Medicine*, ed. MEP. 1996, Suffolk (UK). 151.
12. Group, I.E., *Memory Metal*. 2004, University of Wisconsin System.
13. Turner, T.L., *Dynamic response tuning of composite beams by embedded shape memory alloy actuators*, in *SPIE*. 2000. p. 12.
14. McKelvey, A.L.R., R.O., *Fatigue crack propagation in Nitinol, a shape memory and superelastic endovascular stent material.* J Biomed Mater Res, 1999. **47**(3): p. 301-8.
15. Wayne, J., *Finite Element Analysis.* Encyclopedia of Biomaterials and Biomedical Engineering, 2004: p. 621-629.
16. ADINA, *ADINA System Online Manuals*. 2004.
17. *Zugversuch*, MPA Stuttgart.

Appendix A

Overview of wires for the experimental SMA wire tensile test

Experimental tests were performed for different Nitinol wire samples. Table A.1 gives an overview of the tested wires and the testing conditions. Additionally, the parameters for the program adjustment are listed.

Tab.A.1: Tested wires for the experimental wire tensile test and setting parameter for the program adjustment

Experimental Wire tensile test-Tested wires and setting parameter												
Wire	experiment#	repeat	behaviour	length [mm]	Diameter [µm]	Testing T [°C]	Force [N]	apply break?	speed [mm/min]	cycles	stent wire	heat set?
ARM0137	3	1	linear	100	50	37	3,2	y	102,54	31/2	n	n
ARM0137	4-7	1	linear	100	50	37	0,7	n	102,54	31/2	n	n
ARM0137	8-11	2	linear	100	50	37	0,7	n	30	31/2	n	n
ARM0137	12-15	3	linear	100	50	50	0,7	n	30	31/2	n	n
ARM0137	16-19	4	linear	100	50	50	1,2	n	30	31/2	n	n
ARM0137	20	5	linear	100	50	50	1,2	y	10	31/2	n	n
											n	n
Lot #035906	21-24	1	linear	100	50	37	0,7	n	102,54	31/2	n	n
Lot #035906	25-26	2	linear	100	50	37	1,2	n	102,54	31/2	n	n
Lot #035906	27	3	linear	100	50	37	1,2	n	1	31/2	n	n
ARM0103	28	1	linear	40	50	37	0,7	n	1	31/2	y	y
ARM0103	29-32	2	linear	40	50	37	0.7	n	102.54	31/2	y	y
ARM0103	33-36	3	SE	40	50	37	1,2	n	102.54	31/2	y	y
ARM0103	37	4	SE	40	50	37	1,2	n	1	31/2	y	y
ARM0103	38	5	SE	40	50	37	3	y	102.54	31/2	y	y
											y	y
ARM0002	39	1	linear	100	76,2	37	0.7	n	102.54	31/2	y	y
ARM0002	40	2	linear	100	76,2	37	1,2	n	102.54	31/2	y	y
ARM0002	41	3	linear	100	76,2	37	1,4	n	102.54	31/2	y	y
ARM0002	42	4	linear	100	76,2	37	1,8	n	102.54	31/2	y	y
ARM0002	43	5	linear	100	76,2	37	2,5	n	102.54	31/2	y	y
ARM0002	44	6	SE	100	76,2	37	3	n	102.54	31/2	y	y
ARM0002	45	7	SE	100	76,2	37	3	n	1	31/2	y	y
ARM0002	46	8	SE	100	76,2	37	3	n	1	31/2	y	y
ARM0002	47	9	SE	100	76,2	37	3	y	1	31/2	y	y
											y	y
ARM0114	1	1	SE	100	45	37	1,2	n	102.54	31/2	y	y
ARM0114	2	2	SE	100	45	37	1,2	y	102.54	31/2	y	y
ARM0114	3	1	SE	100	45	37	1,2	y	102.54	31/2	y	y
											y	y
ARM0138	1	1	SE	100	50	37	1,2	y	102.54	31/2	y	y
ARM0138	2	1	plastic	100	50	37	1,2	y	102.54	31/2	y	y
ARM0138	3	1	plastic	100	50	37	1,2	y	102.54	31/2	y	y
ARM0138	4	1	plastic	100	50	37	1,2	y	102.54	31/2	y	y
											y	y
ARM0102	1	1	linear	100	50	37	1,2	n	102.54	31/2	y	y
ARM0102	2	2	SE	100	50	37	1,4	n	102.54	31/2	y	y
ARM0102	3	3	SE	100	50	37	1,4	y	102.54	31/2	y	y
ARM0102	4	1	SE	100	50	37	1,4	y	102.54	31/2	y	y
ARM0102	5	1	SE	100	50	37	1,4	y	102.54	31/2	y	y
ARM0102	6	1	SE	100	50	37	1,4	y	2	31/2	y	y
ARM0102	7	1	SE	100	50	37	1,4	y	2	31/2	y	y
ARM0102	8	1	SE	100	50	37	1,4	y	2	31/2	y	y
ARM0102	9	1	SE	100	50	37	1,4	y	102.54	200	y	y
ARM0102	10	1	SE	100	50	37	1,4	y	102.54	200	y	y
ARM0102	11	1	SE	100	50	21	1,4	y	102.54	31/2	y	y
ARM0102	12	1	SE	100	50	10	1,4	y	102.54	31/2	y	y
ARM0102	13	1	SE	100	50	0	1,4	y	102.54	31/2	y	y

Appendix B

Instructions to compile user subroutine DLL

The user subroutine has to be compiled into a dll-file (dynamic link library file) which must be placed in the same directory as the executable program. To run a program with the dll containing the new user subroutines, the new dll build and replace the original dll in the %ADINAHOME%\bin directory. [16]

All the FORTRAN source code for programming the own user subroutines are in the %ADINAHOME%\usrdll directory. The directory also contains the Makefiles for building the dlls.

Compaq Visual Fortran 6.6A is required for compiling a new dll-file.

The following steps are required for replacing the dll-file:

- Backup of the original dll-file in the %ADINAHOME%\bin directory.
- Modification of the FORTRAN source files in the %ADINAHOME%\usrdll directory.
- Compilation of new dll-file which includes the modifications:
    - First, the Fortran environment is set up in a Command Prompt window by issuing the following command:

      ...\DF98\bin\dfvars

      "...\" is substituted with the full path name where Compaq Visual Fortran is installed.
    - Compilation of adusr.dll using the following command:

      nmake /f Makefile. adusr

- Copy of the new dll-file has to be inserted into the %ADINAHOME%\bin directory.